Perspective: Thermal and thermoelectric transport in molecular junctions

Longji Cui,[1,a)] Ruijiao Miao,[1,a)] Chang Jiang,[1] Edgar Meyhofer,[1,b)] and Pramod Reddy[1,2,c)]
[1]*Department of Mechanical Engineering, University of Michigan, Ann Arbor, Michigan 48109, USA*
[2]*Department of Materials Science and Engineering, University of Michigan, Ann Arbor, Michigan 48109, USA*

(Received 1 November 2016; accepted 7 February 2017; published online 1 March 2017)

With the advent of molecular electronics, tremendous attention has been paid towards understanding the structure-function relationship of molecular junctions. Understanding how heat is transported, dissipated, and converted into electricity in molecular junctions is of great importance for designing thermally robust molecular circuits and high-performance energy conversion devices. Further, the study of thermal and thermoelectric phenomena in molecular junctions provides novel insights into the limits of applicability of classical laws. Here, we present a review of the computational and experimental progress made in probing thermoelectric effects, thermal conduction, heat dissipation, and local heating/cooling in self-assembled monolayer and single molecule junctions. We also discuss some outstanding challenges and potential future directions. *Published by AIP Publishing.* [http://dx.doi.org/10.1063/1.4976982]

I. INTRODUCTION

The intriguing idea[1] of building electrical components and interconnects using single molecules has greatly inspired researchers over the past several decades and led to the emergence of the field of "molecular electronics." Transport characteristics of junctions of molecules between electrodes (Fig. 1(a)), called molecular junctions (MJs), have been extensively explored to investigate the feasibility of creating molecular devices with desirable transport characteristics. Both experimental and theoretical work has shown that MJs can indeed be employed to achieve unique and interesting charge transport characteristics.[2–9] Owing to technical and computational advancements over the last decade, energy (thermal) transport and conversion properties of MJs have attracted considerable attention.[10–16] Fundamentally, probing thermal transport in MJs is useful to understand the limits to the applicability of classical theories at the nanoscale. Moreover, such studies are also essential for future practical applications of MJs in electronic devices and for developing high-efficiency energy conversion devices. For example, it has been computationally proposed that by carefully designing MJs, it is possible to achieve very efficient thermoelectric energy conversion.[17–20] Furthermore, single molecular chains are also expected to feature ultrahigh thermal conductivities, in strong contrast to the relatively poor thermal conductivity of polymer materials,[21,22] indicating that a more detailed understanding of thermal transport in such molecules may enable the creation of polymer based materials with high thermal conductivity.

In this article, we review current understanding of thermal and thermoelectric properties of MJs. Insights obtained from both theoretical and experimental investigations of both self-assembled monolayer (SAM) based and single molecule based MJs will be described. This paper is organized as follows: in Section II, we briefly introduce the Landauer formalism that is used to describe transport in MJs; subsequently in Section III, we review the theoretical and experimental advancements in studying thermoelectric effects in MJs; in Section IV, recent work on heat conduction, heat dissipation, and local heating/cooling of MJs will be discussed. Finally, we conclude by highlighting some open questions in the field.

II. LANDAUER THEORY OF QUANTUM TRANSPORT

A. Electrical conductance

Landauer's seminal work[23] which relates electrical conductance to electron transmission is widely used for describing transport in MJs.[24–26] Within the Landauer formalism (Fig. 1(b)), the electrical current (I) at finite bias (V) is given by[26]

$$I = \frac{2e}{h}\int_{-\infty}^{+\infty}(f_L - f_R)\tau(E)dE, \tag{1}$$

where $f_{L/R}$ is the Fermi-Dirac distribution of the left/right electrodes and $\tau(E)$ is the energy (E) dependent transmission function, which describes the probability of electron transmission through the MJ. Under the small-bias and low-temperature approximations, Eq. (1) can be simplified to yield $I/V = G_e = (2e^2/h)\tau_{E=E_F}$, where E_F is the Fermi energy (chemical potential). Interestingly, for one fully open channel ($\tau_{E=E_F} = 1$), the electrical conductance is given by $G_e = G_0 = 2e^2/h = 1/(12.9\ \ k\Omega)$, which is the quantum of electrical conductance.

B. Seebeck coefficient

The thermoelectric properties of MJs can also be described within the Landauer formalism (Fig. 1(c)). Specifically, when a temperature difference (ΔT) is applied across

a)L. Cui and R. Miao contributed equally to this paper.
b)meyhofer@umich.edu
c)pramodr@umich.edu

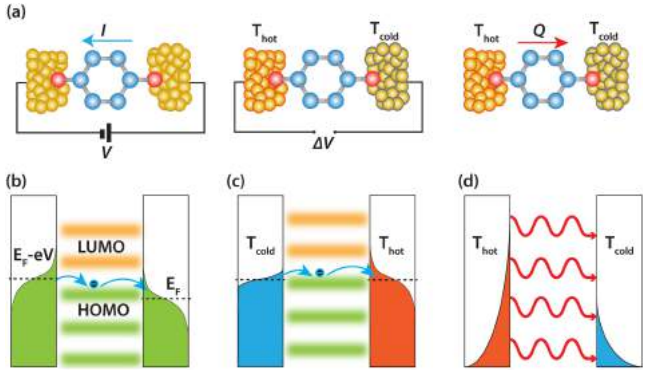

FIG. 1. Schematics describing charge, thermoelectric, and thermal transport in molecular junctions (MJs). (a) An organic molecule bridged between two electrodes to form a single MJ. Left: electrical conductance measurement scheme. Middle: thermoelectric (Seebeck coefficient) measurement scheme. Right: thermal conductance measurement scheme. (b) Electric currents in a MJ are driven by a difference in the Fermi-Dirac distributions in the electrodes arising from an applied bias (V). (c) Thermoelectric transport under a temperature difference ($T_{hot} - T_{cold}$). The sign of the Seebeck coefficient (S) is determined by the alignment of the HOMO and LUMO levels of the MJ with respect to the Fermi level of the electrodes. (d) Heat transport due to phonons when a temperature differential is applied to the electrodes; the Bose-Einstein distributions for phonons in the hot and cold electrodes are shown as red and blue shaded regions, respectively.

a MJ, an open-circuit voltage (ΔV) develops across the junction (Fig. 1(c)). The Seebeck coefficient (S) is given by $S = -\Delta V/\Delta T$ and can be related to the transmission function by[27,28]

$$S = -\frac{\pi^2 k_B^2 T}{3\,|e|}\frac{\partial \ln(\tau(E))}{\partial E}\bigg|_{E=E_F}. \tag{2}$$

It is clear from the above expression, which is valid if the transmission function is smooth and slowly varying in an energy range of $\sim k_B T$ around E_F, that the slope of the transmission function at E_F determines the sign and magnitude of the Seebeck coefficient.

C. Thermal conductance

Thermal transport through MJs (Fig. 1(d)) can also be described within the Landauer formalism. The electronic heat current ($J_{electrons}$) and the phononic heat current ($J_{phonons}$), when a temperature difference ΔT is applied, are given by[23,29]

$$J_{electrons} = \frac{2}{h}\int_{-\infty}^{\infty}\left(E - E_f\right)\tau(E)\left(f_L - f_R\right)dE \tag{3}$$

and

$$J_{phonons} = \int_{0}^{\infty}(h\upsilon)\tau_{ph}(\upsilon)\left(g_L - g_R\right)d\upsilon, \tag{4}$$

where υ is the phonon frequency and $\tau_{ph}(\upsilon)$ is the transmission function for phonons and g_L and g_R denote the Bose-Einstein distributions for the left and the right thermal reservoirs, respectively, and depend on the temperature of the electrodes.

D. Heat dissipation

When a voltage bias V is applied across a MJ, it results in both an electrical current (I) and heat dissipation in the junction. Within the Landauer approach, it can be shown that when the heat dissipation in the molecular region is negligible, i.e., when transport is elastic, the heat dissipation in the left and right electrodes, Q_L and Q_R, respectively, is given by[30,31]

$$Q_L = \frac{2}{h}\int_{-\infty}^{\infty}(\mu_L - E)\tau(E)\left(f_L - f_R\right)dE \tag{5}$$

and

$$Q_R = \frac{2}{h}\int_{-\infty}^{\infty}(E - \mu_R)\tau(E)\left(f_L - f_R\right)dE, \tag{6}$$

where $\mu_{L/R}$ represent the chemical potentials of the left/right electrodes, respectively.

In Sec. III, we describe thermoelectric phenomena in MJs. We begin by describing the reasons why thermoelectric properties of MJs are interesting. Subsequently, we describe theoretical and computational studies that highlight the potential of MJs for thermoelectric energy conversion. Finally, we describe the currently available experimental techniques and the progress to date in probing thermoelectric effects of MJs.

III. THERMOELECTRIC TRANSPORT IN MOLECULAR JUNCTIONS

Thermoelectric materials have long been employed as solid-state heat engines that convert heat into electricity. The energy conversion efficiency is represented by a dimensionless quantity called the figure of merit (ZT) which is defined as $ZT = \frac{S^2\sigma T}{\kappa}$, where S is the Seebeck coefficient (also called thermopower), σ is the electrical conductivity, κ is the thermal conductivity, and T is the absolute temperature. Analogous to bulk materials, the efficiency of a MJ in converting heat into electricity is quantified by

$$ZT = \frac{S^2 G_e T}{G_{th}}, \tag{7}$$

where G_e and G_{th} represent the electrical and thermal conductances, respectively. The energy conversion efficiency (η) of a MJ monotonically increases with ZT and is given by

$$\eta = \eta_C\frac{\sqrt{1+ZT}-1}{\sqrt{1+ZT}+{}^{T_C}/_{T_H}}, \tag{8}$$

where T_H and T_C are the temperature of the hot side and the cold side, respectively, and $\eta_C = 1 - {}^{T_C}/_{T_H}$ is the Carnot efficiency which represents the upper limit to energy conversion efficiency that any heat engine can achieve. It can be seen from Eq. (8) that achieving high energy conversion efficiency requires a large ZT which in turn can be obtained if MJs feature a large thermopower and electric conductance, and a small thermal conductance. Given the results in Eqs. (1), (2), and (7) it is clear that large values of ZT can be achieved if MJs simultaneously feature a large value of $\tau(E)$ and a large gradient of the transmission $\partial\tau/\partial E$ at the chemical potential (E_F).

A. Computational results

One of the first works to explore thermoelectric properties in MJs was by Paulsson and Datta,[28] where they analyzed the

thermoelectric current and voltage of benzenedithiol (BDT) based MJs. Their findings suggested that the thermoelectric current and voltage output of BDT MJs were large enough to be measured and insensitive to the molecule-electrode coupling details. Further, their work suggested that the relative position of the HOMO (highest occupied molecular orbital) and LUMO (lowest unoccupied molecular orbital) with respect to the Fermi energy plays an important role in determining the sign of the Seebeck coefficient, indicating that thermoelectric measurements of MJs can reveal important information about the electronic structures of MJs.

Subsequently, several groups theoretically studied the thermoelectric properties of MJs to explore the feasibility of achieving high *ZT*.[17,18,28,32–45] For example, Finch *et al.*[17] presented a computational study for CSW-479-bipyridine MJs with gold electrodes (Fig. 2(a)). They showed that by tuning the orientation of a side group with respect to the molecular backbone, the thermopower could be dramatically enhanced, resulting in a large *ZT* value. They attributed this enhancement to Fano resonances,[46] which arise from the presence of degenerate energy levels in the molecular backbone and the side groups. Specifically, they found that the transmission function showed a peak, which was shifted towards the Fermi energy by controlling the angular orientation of the side group.

Bergfield *et al.*[18] investigated polyphenyl ether (PPE) molecules bridged between gold electrodes (Fig. 2(b)). Their work suggested that a sharp peak in the transmission function near the Fermi energy could arise from quantum interference effects,[41,47,48] and thus could lead to a large Seebeck coefficient. Further, they showed that by increasing the number of phenyl rings in the molecule, very high values of *ZT* (>4) were achievable.

Besides modifying the shape of transmission function by means of quantum interferences, recent work has also found that spin-crossover could be used to tune the charge transport[49–51] and thermoelectric properties[52] of molecule-ferromagnetic metal junctions. For example, Ghosh *et al.*[52] studied a spin-crossover molecule Fe(2-(1H-pyrazol-1-yl)-6-(1H-tetrazole-5-yl)pyridine)$_2$ ([Fe(L)$_2$]) which has a sharp

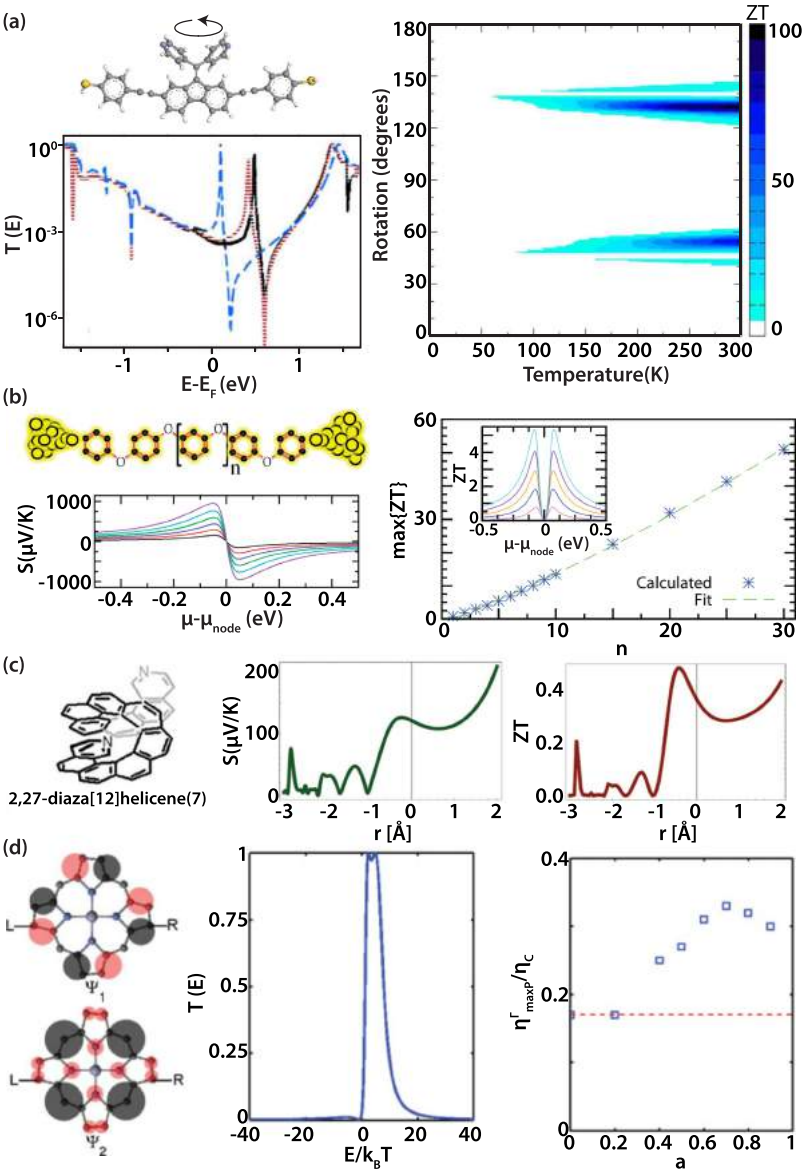

FIG. 2. Theoretical proposals for enhancing thermoelectricity in MJs. (a) Results for CSW-479-bipyridine molecule.[17] Left top: schematic of the molecule with a side group which can rotate around the C–C bond connecting it to the molecule. Left bottom: transmission function when the side group is rotated. Right: calculated *ZT* with respect to rotation angle and temperature. Darker color indicates higher *ZT*. Reproduced with permission from C. M. Finch, V. M. Garcia-Suarez, and C. J. Lambert, Phys. Rev. B **79**, 033405 (2009). Copyright 2009 American Physical Society. (b) Computed thermoelectric properties of polyphenyl ether (PPE) molecules.[18] Schematic of the molecule is shown on top left with length denoted as *n*. Left bottom: Seebeck coefficient vs chemical potential from $n = 1$ (black line) to $n = 7$ (purple line). Right: maximum *ZT* plotted as a function of *n*. Inset: *ZT* vs. chemical potential, where the maximum *ZT* value increases with *n*. Reproduced with permission from J. P. Bergfield, M. A. Solis, and C. A. Stafford, ACS Nano **4**, 5314 (2010). Copyright 2010 American Chemical Society. (c) Helicene MJs.[20] Left: schematic of helicene molecule subject to mechanical stretching/compression. Middle: Seebeck coefficient with respect to stretching/compressing distance. $r < 0$ indicates compression and $r > 0$ stretching. Right: plot of calculated *ZT*. Reproduced with permission from Vacek *et al.*, Nanoscale **7**, 8793 (2015). Copyright 2015 Royal Society of Chemistry. (d) Analysis of high power output energy conversion.[44] Left: schematic of zinc porphine molecule with sketching of wave function of the two degenerate levels. Light/dark shade indicates positive/negative magnitude of wave function. Middle: plot of the transmission function. The low-energy tail is eliminated. Right: plot of efficiency at maximum output power (η^{Γ}_{maxP}) in units of Carnot efficiency (η_C) as a function of the difference between the coupling strength of two levels (a, defined in Eq. (10)). Reproduced with permission from Karlstrom *et al.*, Phys. Rev. B **84**, 113415 (2011). Copyright 2011 American Physical Society.

transition from a low-spin (LS) state to a high-spin (HS) state upon elevating the temperature of the junction, and both spin and electron contributed to the thermoelectric current. In this work, ZT for the HS state (at 350 K) was found to be 4 times higher than the ZT for the LS state (at 250 K).

Vacek *et al.*[20] studied thermoelectric properties in helicene MJs when the helical shaped junctions are mechanically stretched or compressed (Fig. 2(c)). Their calculations showed that when the molecular junction is compressed, a significant enhancement of electrical conductance and a sign-change in thermopower, originating from the change in the overlap of the wave functions of nearest atoms, is expected along with a concomitant increase in ZT. Upon stretching, the ZT value was found to first decrease and subsequently increase. They suggested that the idea of mechanically controlling electric conductance and thermopower could also be applied to other non-planar shaped molecules including cycloparaphenylenes, cyclacenes, ball-like molecules, carbon cages, tailored fullerenes, fullerene cages, and short DNA molecules.

As described above several computational studies have suggested that it may be feasible to perform thermoelectric energy conversion at efficiencies close to the Carnot limit (i.e., very high values of ZT). However, it is well know that operation close to the Carnot limit implies operation and the reversible limit and therefore, the power output is negligible. In practice, as has been highlighted in recent works,[44,53,54] it is essential to understand the relationship between efficiency and power output under irreversible conditions. The Curzon-Ahlborn (CA) limit, which describes the thermodynamically maximum efficiency of a heat engine operating under conditions where the power output is maximized, is therefore of great interest. The maximum efficiency of a heat engine operating at maximum output power is given by $\eta_{CA} = \frac{\eta_C}{2} + \frac{\eta_C^2}{8} + O\left(\eta_C^3\right) + \cdots$, where $\eta_{CA}(\eta_C)$ is the Curzon-Ahlborn (Carnot) efficiency. To achieve this maximum output power, the transmission function of MJs has to be rationally designed.

In this regard, Nakpathomkun *et al.*[19] studied a low-dimensional system with an approximately Lorentzian shape transmission function, which is given by

$$\tau(E) = \frac{(\Gamma/2)^2}{(E - E_o)^2 + (\Gamma/2)^2}, \tag{9}$$

where E_0 is the center position of the Lorentzian and Γ is the full width at half of maximum of $\tau(E)$. They showed that by carefully choosing Γ and the relative position of E_0 and E_F, the output power can be optimized. However, they also showed that the Curzon-Ahlborn limit cannot be reached with a Lorentzian shaped $\tau(E)$ due to the low-energy tail, which permits a detrimental electric current in a direction opposite to the thermoelectric current.

To overcome this challenge, Karlstrom *et al.*[44] took advantage of the quantum interference in a two-level system (Fig. 2(d)) where the transmission function is expressed as

$$\tau(E) = \Gamma^2 \left| \frac{1}{(E - E_F) + E_1 + i\Gamma} - \frac{a^2}{(E - E_F) + E_2 + ia^2\Gamma} \right|, \tag{10}$$

where the energy levels E_1 and E_2 are located on the same side of E_F, and the coupling strengths of the two energy levels to the electrodes differ by a factor of a^2. When $E_2 = a^2 E_1$, $\tau(E)$ is zero at E_F and is large for a finite range of energies above E_F. This implies that $\tau(E)$ has a large gradient at E_F and a finite width so that the system can operate with large power output. They further showed that the efficiency of such a system can be very close to the CA-limit. Finally, they suggested that the desired transmission function can be realized in Au–zinc porphine–Au MJs.

Taken together, computational work on the thermoelectric efficiencies of MJs suggests various strategies to achieve energy conversion at very high efficiencies (close to the Carnot limit) and large power outputs (close to the CA-limit). Key to achieving this goal is to develop strategies for achieving transmission functions that show rapid variations at the Fermi energy (e.g., delta/step shaped functions or an asymmetric Lorentzian-like transmission function[55]). Other approaches to tune the transmission function include redox control of the quantum interference within phase coherent molecular wires,[56] variation of the transition metal-center in porphyrin-based conjugated molecules,[57] and creating π-π overlap between planar aromatic anchor groups and electro-burnt graphene electrodes.[58] In the following, we will discuss past experimental work on probing the thermoelectric properties of MJs.

B. Experiments

Several groups have experimentally quantified the thermoelectric properties of MJs. In Table I, we summarize the results obtained so far (to the best of our knowledge). Below, we first provide a brief discussion of experimental techniques that were developed to measure the thermoelectric properties of MJs in two-terminal configurations, i.e., techniques that enable the measurement of a voltage output from junctions created by trapping molecules between a hot and a cold electrode. Subsequently, we review experimental work that elucidated the dependence of thermoelectric properties of MJs on molecular length, end groups, molecular structures and conformation, electrode materials, and temperature. Finally we discuss three-terminal techniques that enable tuning of the thermoelectric properties of MJs.

1. Two-terminal thermoelectric measurements

Some of the initial experimental studies of thermoelectric properties of MJs were performed by Reddy *et al.*[59] In performing these studies the authors adapted a STM based technique called the STM break-junction (STMBJ) technique that was originally developed by Xu and Tao[60] for probing electrical transport in MJs (Fig. 3(a)). Since the electrical and thermoelectric properties of MJs are pivotal to thermoelectric energy conversion, we first introduce the STMBJ technique and then describe how it was modified[59] for single-molecule thermoelectric measurements.

In the STMBJ technique a voltage bias is applied between a sharp tip of an STM (typically made of Au) and a Au substrate covered with a monolayer of molecules that are chemically bound to the substrate via endgroups such as thiols (–SH).

TABLE I. List of experimental results of molecular junctions.

Molecule	Chemical structure	Conductance (G/G_0)	Thermopower S ($\mu V/K$)	Electrodes	Technique
1,4-Benzenedithiol (BDT)		0.012 ± 0.0009	3.07 ± 12.6 (T_{ave} = 99 K) 5.08 ± 1.83 (T_{ave} = 157 K) 6.38 ± 1.65 (T_{ave} = 219 K) 9.26 ± 1.77 (T_{ave} = 277 K) 9.86 ± 2.26 (T_{ave} = 318 K)	Au–Au	STM Varied temperature[98]
1,4-Benzenedithiol (BDT)	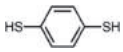	0.01	1.4	Au–Au	MCBJ[176]
1,4-Benzenedithiol (BDT)	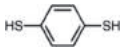	0.01	7.44 ± 0.5 −12.1 ± 1.3	Au–Au Ni–Ni	STM[97]
1,4-Benzenedithiol (BDT)		0.01	11	Au–Au	MCBJ[177]
1,4-Benzenedithiol (BDT)		0.011	15 ± 4	Au–Au	MCBJ[168]
1,4-Benzenedithiol (BDT) 4,4′-dibenzenedithiol (DBDT) 4,4″-tribenzenedithiol (TBDT)	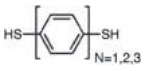		8.7 ± 2.1 12.9 ± 2.2 14.2 ± 3.2	Au–Au	STM[59]
1,4-Benzenedithiol (BDT) 4,4′-dibenzenedithiol (DBDT) 4,4″-tribenzenedithiol (TBDT)	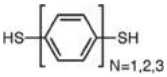		7.7 ± 0.5 10.8 ± 0.6 15.1 ± 0.9	Au–Au	STM[76]
2′,5′-Dimethyl-4,4″-tribenzenedithiol (DMTBDT)	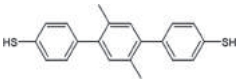		15.9 ± 2.5		
1,1′,4′,1″-Terphenyl-4-thiol (TPT)			16.9 ± 1.4	Au–Au	CP-AMFSAM[63]
1,4-n-Benzenethiol (n-BT) (n-1,2,3,4)	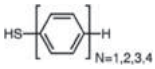		8.1 ± 0.8 13.6 ± 1.2 17.0 ± 1.0 21.0 ± 1.3	Au–Au	CP-AMFSAM[85]
1,4-n-Benzenedithiol (nBDT) (n = 1,2,3)	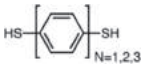		9.8 ± 0.6 11.7 ± 1.3 15.4 ± 1.0		
1-Tribenzenecyanide (TBCN)	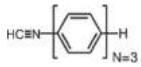		−1.0 ± 0.4		
n-Alkanedithiol (ADT) (n = 2,3,4,5,6,8)	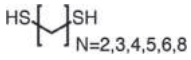		6.8 ± 0.2 5.5 ± 0.1 5.2 ± 0.4 4.9 ± 0.2 3.3 ± 0.1 2.4 ± 0.4	Au–Au	STM[75]
1,4-n-Phenylenediamine (PDA) (n-1,2,3)			2.3 ± 0.3 4.9 ± 1.9 6.4 ± 0.4		

TABLE I. (*continued.*)

Molecule	Chemical structure	Conductance (G/G_0)	Thermopower S ($\mu V/K$)	Electrodes	Technique
1,4-Bis((trimethylstannyl)methyl)-n-phenyl (n = 1,2,3,4)	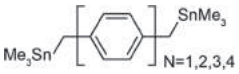	0.9 0.1 0.014 0.002	2.4 14.3 20.9 23.9	Au–Au	STM[77]
1,6-Bis(trimethylstannyl)-n-alkanes (n = 6,8,10)	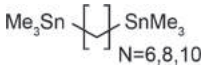	0.014 0.002 0.0003	5.0 5.6 5.6		
n-Alkanethiol (n = 1,2,3,4) and thiocyanate	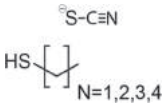		2.6 1.5 0.3 −3.7 −1.3	Au	Nanocrystal array[178]
n-Alkanedithiol (n = 1,2,3,5,7)	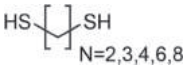		−1.4 −2.4 −1.5 −0.8 −0.5		
n-Oligophenyldithiol (n = 1,2,3)			17 38 26		
n-Oligophenyldiamine (n = 1,2,3)		· · · · · · 1.7×10^{-4}	2.1 6.3 8.7	Ag–Ag	STM[179]
4,4′-bipyridine	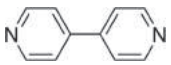	4×10^{-4} (high G) 1×10^{-4} (low G)	−8.4 −7.5	Au–Au	STM[180]
1,2-Di(4-pyridyl)ethylene (BPE)	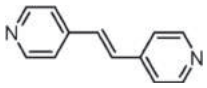	2.8×10^{-4} (high G) 7.5×10^{-5} (low G)	−10.1 −9.3		
1,4-n-Phenylenediamine (n = 1, 2, 3)	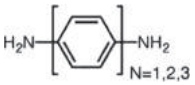	6.25×10^{-3} 1.10×10^{-3} 1.6×10^{-4}	3.1 7.9 10.4		
4,7-Dithiophenyl-2,1,3-benzothiadiazole-3,3-dithiol (DTBTDT)	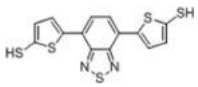	9.2×10^{-3}	15.46 ± 0.15	Au–Au	STM[181]
1,4-Butanedithiol (C4)		4.5×10^{-3}	2.11 ± 0.11		
1,6-Hexanedithiol (C6)		6.2×10^{-4}	5.55 ± 0.13		
1,4-Biphenyldithiol (BPDT)	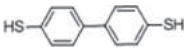	5.2×10^{-3}	8.35 ± 0.23		
4,4-Dimercaptostilbene (DMS) 5.2	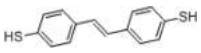	7.5×10^{-3}	7.92 ± 0.14		
4,4′-Diaminostilbene	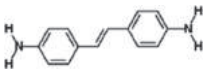	0.63×10^{-3}	13.0 ± 7.0	Au–Au	STM[62]
Bis-(4-aminophenyl)acetylene		0.57×10^{-3}	9.7 ± 6.1		
1,5-Bis-(diphenylphosphino)pentane		0.39×10^{-3}	1.1 ± 4.1		
4,4′-Bipyridine	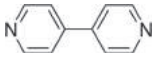	0.68×10^{-3}	−9.5 ± 4.3		
1,2-Di(4-pyridyl)ethylene	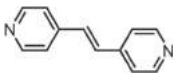	0.24×10^{-3}	−12.3 ± 9.1		

TABLE I. (*continued.*)

Molecule	Chemical structure	Conductance (G/G_0)	Thermopower S (μV/K)	Electrodes	Technique
S,S′-Thiophene-2,5-diyl diethanethioate (T1)	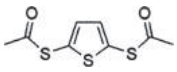	0.0075	6.83		
S,S′-Thiophene-2,5-diylbis (methylene)-diethanethioate (TA2)	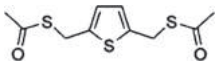	0.0035	3.01		
S,S′-2,20-(Thiophene-2,5-diyl)bis (ethane-2,1-dyil)-diethanethioate (TA3)	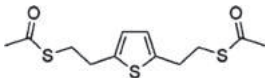	0.002	2.2	Au–Au	STM[182]
S,S′-([2,20-Bithiophene]-5,50-diyl)diethanethioate (OT2)	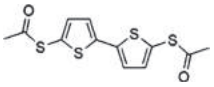	0.0031	7.49		
S,S′-([2,2: 50,200-Terthiophene]-5500-diyl)-diethanethioate (OT3)	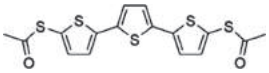	0.0007	14.84		
Oligomers of thiophene-1,1-dioxide (TDOn, n = 1, 2, 3, 4)	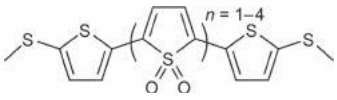	9×10^{-4} 5×10^{-4} 2×10^{-4} 6×10^{-5}	7.3 6.4 2.4 −22.1	Au–Au	STM[183]
Fullerene C_{60}		7.0×10^{-4} 2.5×10^{-4} 2.0×10^{-3}	−8.9 ± 2.2 −14.5 ± 1.2 −29.6 ± 3.4	Substrate-tip Au–Pt Au–Au Au–Ag	STM[96]
[6,6]-phenyl-C_{61}-butyric acid methyl ester (PCBM)		1.3×10^{-3} 2.5×10^{-3}	−7.6 ± 3.2 −16.4 ± 1.6 −30.0 ± 2.6	Au–Pt Au–Au Au–Ag	
Fullerene C_{70}		6.2×10^{-4} 6.2×10^{-4} 1.6×10^{-3}	−8.4 ± 1.9 −20.1 ± 1.4 −33.1 ± 1.8	Au–Pt Au–Au Au–Ag	
Fullerene C_{60}		0.1	−18 ± 6.84	Au–Au	STM[80]
Fullerene C_{60} dimer		1.8×10^{-3}	−33 ± 11.88		
Fullerene C_{60}		0.2	−16.1 ± 0.5 −12.5 ± 1.2	Au–Au Ni–Ni	STM[97]
Biphenyl-4,4′-dithiol (BPDT)	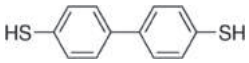	0.006-0.003	7.7 (V_G = −8 V) 7.4 (V_G = −4 V) 6.6 (V_G = 0 V) 5.8 (V_G = −4 V) 5.6 (V_G = −8 V)	Au–Au	EBJ electrostatic gating[111]
Fullerene C_{60}		0.43-0.65	−30 (V_G = −8 V) −42 (V_G = −4 V) −34 (V_G = 0 V) −32 (V_G = 4 V) −12 (V_G = 8 V)		

TABLE I. (*continued.*)

Molecule	Chemical structure	Conductance (G/G_0)	Thermopower S ($\mu V/K$)	Electrodes	Technique
Fullerene C_{82}		0.2	−22.7 ± 0.9		
Endohedral fullerene $Gd@C_{82}$		0.2	−31.6 ± 1.2	Au–Au	STM[90]
Endohedral fullerene $Ce@C_{82}$		0.2	−30.0 ± 1.0		
Endohedral fullerene $Sc_3N@C_{80}$	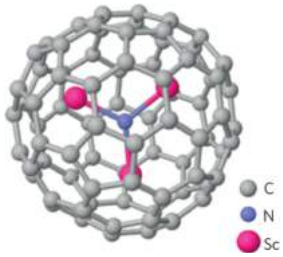	0.05	−25~25	Au–Au	STM varied separation between tip and substrate. Varied molecule orientation.[91]
Double strand DNA with GC sequences only	$A(CG)_3T$	0.0067	1.4 ± 0.2		
	$A(CG)_4T$	0.0053	0.8 ± 0.2		
	$A(CG)_5T$	0.0043	1.0 ± 0.2		
	$A(CG)_6T$	0.0038	0.6 ± 0.2		
	$A(CG)_7T$	0.0031	0.8 ± 0.2		
Double strand DNA inserted with AT sequences	ACGC**A**GCGT	0.0049	5.0 ± 0.3	Au–Au	STM[79]
	ACGC**AT**GCGT	0.0044	5.9 ± 0.4		
	ACGC**ATA**GCGT	0.0027	6.5 ± 0.8		
	ACGC(**AT**)$_2$GCGT	0.0017	7.9 ± 0.5		
	ACGC(**AT**)$_2$**A**GCGT	0.0021	4.9 ± 0.2		
	ACGC(**AT**)$_3$GCGT	0.0022	2.0 ± 0.2		
	ACGC(**AT**)$_4$GCGT	0.0017	2.0 ± 0.3		

The tip is displaced towards the substrate while the electrical conductance between the tip and the sample is being monitored. This process continues until an electrical contact is established and an electrical conductance of ~5 G_0 or greater is observed (signifying the formation of Au–Au atomic contacts). During this process, in addition to the formation of Au–Au contacts, some molecules stochastically bridge the electrodes (see Fig. 3(b)). Subsequently, the tip is withdrawn from the substrate, while monitoring the electrical conductance. This process results in a scenario where a few molecules bridge the tip and substrate. By further withdrawing the tip, the molecular bridges break successively until there is only one molecule bridging the tip and the substrate. During this withdrawal process the electrical conductance of the tip-molecule-substrate junctions is measured. Typical conductance traces obtained in such an experiment[61] are shown in Fig. 3(c). A substantial number of conductance traces can then be used to analyze and obtain statistically significant information about the electrical properties of MJs.

In order to investigate thermoelectric effects of MJs, the STMBJ techniques are modified so as to enable the application of a temperature difference across the MJs. In Fig. 4(a), a single MJ formed by using the STMBJ technique is depicted. The Au substrate is heated while the STM tip is kept at room temperature by placing it in contact with a large thermal reservoir. Because thermal conductance of the MJ is much smaller (quantified later in this article) than the thermal conductance of the gold STM tip, a tip-substrate temperature difference, ΔT, is readily established.[55,57]

The procedure to measure the Seebeck coefficient involves trapping of multiple molecules between the electrodes by following the procedure described above. Subsequently, the voltage bias and the current amplifier that are used to monitor the current are disconnected and a voltage amplifier is connected to measure the thermoelectric voltage induced by ΔT (see Fig. 4(a)). The tip is slowly withdrawn until all the trapped molecules break off. During this process, the output voltage, ΔV, is continuously monitored. When the last molecule breaks off, the thermoelelctric voltage vanishes. This output voltage ΔV, due to ΔT, is a measure of the Seebeck coefficient and is obtained by $S = -\Delta V/\Delta T$.

Reddy *et al.*[59] employed the above-described STMBJ technique to probe the thermoelectric properties of MJs created from benzenedithiol, dibenzenedithiol, and tribenzenedithiol

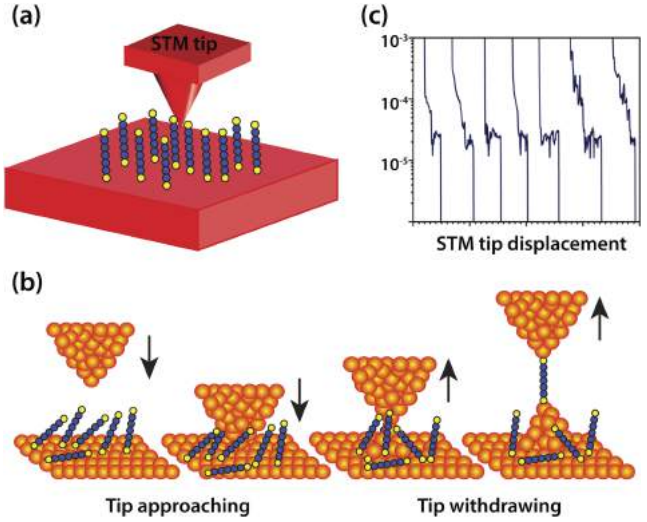

FIG. 3. Schematic of the STM break junction (STMBJ) technique. (a) STM tip is in proximity to a substrate bonded with SAM MJs. (b) The process of trapping a single MJ. STM tip is brought in contact with the substrate. MJs are formed when the STM tip retracts from the substrate until only one molecule bridges the tip and substrate. (c) Representative traces of electrical conductance of the junction during the withdrawal process.[61] Reproduced with permission from W. Lee and P. Reddy, Nanotechnology **22**, 485703 (2011). Copyright 2011 IOP publishing.

molecules and Au electrodes (Fig. 5(a)). These experiments revealed that the Seebeck coefficient of these aromatic MJs is positive and increases monotonically (and approximately linearly) with molecular length.

The STMBJ technique as applied to thermoelectric studies was further improved by Widawsky *et al.*[62] who succeeded in simultaneously recording the electrical conductance and thermopower of single MJs in STMBJ technique by measuring both the zero-bias thermocurrent and the electrical conductance under a small applied bias. Using this method the authors explored several amine–Au linked and pyridine–Au linked MJs. From these measurements they observed a positive Seebeck coefficient for amine–Au linked MJs and a negative Seebeck coefficient for pyridine–Au linked MJs, confirming that transport in amine–Au junctions is HOMO dominated whereas that in pyridine–Au junctions is LUMO dominated.

In addition to the STMBJ technique, a different technique that is based on an atomic force microscope (AFM) was developed by Tan *et al.*[63] to probe thermoelectric effects in SAM based MJs. Briefly, a Au-coated AFM probe made of Si, that is at ambient temperature, is placed in contact with a heated Au substrate that is covered with a monolayer of molecules, while the deflection of the cantilever is continuously monitored and

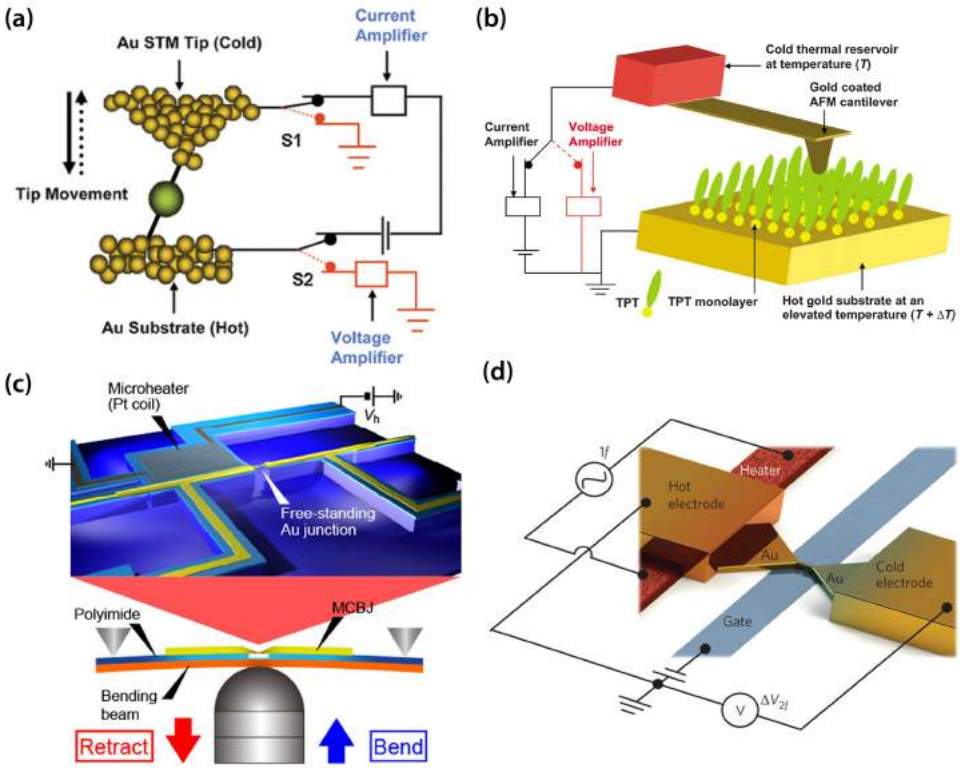

FIG. 4. Schematics of experimental setups for thermoelectric measurements of MJs. (a) STMBJ based setup.[59] The STM tip is kept at ambient temperature while the substrate is heated up. Connections to the current and voltage amplifiers are made at different times to measure the thermoelectric voltage across the junctions. Reproduced with permission from Reddy *et al.*, Science **315**, 1568 (2007). Copyright 2007 AAAS. (b) CP-AFM based setup.[63] The AFM cantilever is in contact with a reservoir at temperature T while the Au substrate is heated to an elevated temperature $T + \Delta T$. Reproduced with permission from A. Tan *et al.*, Appl. Phys. Lett. **96**, 013110 (2010). Copyright 2010 AIP Publishing. (c) MCBJ setup.[74] A free-standing Au junction is created by bending the substrate. Temperature differentials between the electrodes are established via an integrated Pt coil micro-heater. A polyimide layer insulates the Au electrodes from the bending substrate. Reproduced with permission from Tsutsui *et al.*, Sci. Rep. **5**, 11519 (2015). Copyright 2015 Macmillan publishers Ltd. (d) EBJ setup.[111] A gate electrode is used to tune the electronic structure of the junction. One of the electrodes is heated by applying a sinusoidal electric current at frequency f through an integrated heater, resulting in a temperature difference and a thermoelectric voltage output at frequency $2f$. Reproduced with permission from Kim *et al.*, Nat. Nanotechnol. **9**, 881 (2014). Copyright 2014 Macmillan Publishers Ltd.

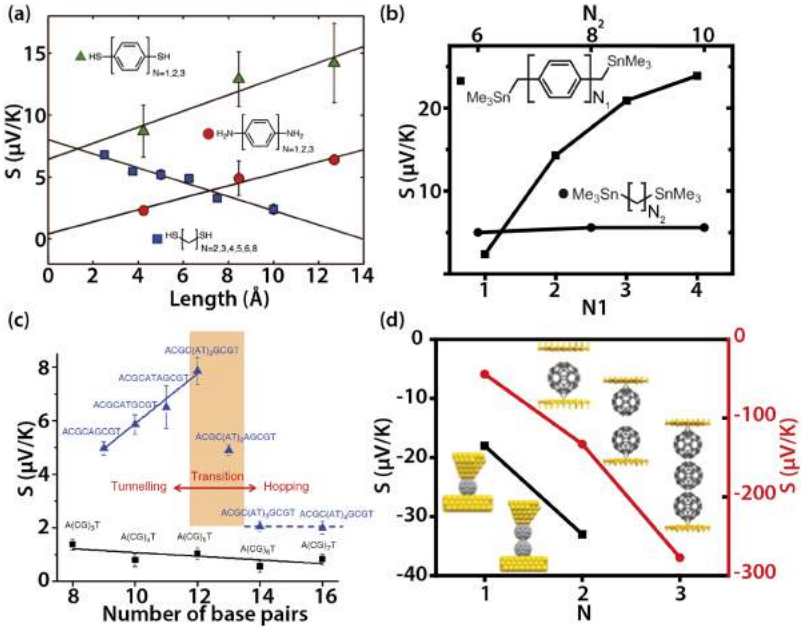

FIG. 5. Length dependence of the Seebeck coefficient of MJs. (a) Seebeck coefficient of phenylenedithiol (green triangle), phenylenediamine (red circle), and ADT (blue square) molecular junctions with respect to molecular length.[75] Reproduced with permission from Malen *et al.*, Nano Lett. **9**, 1164 (2009). Copyright 2009 American Chemical Society. (b) Thermopower of $SnMe_3$ terminated polyphenyl (square, N_1) and $SnMe_3$ terminated alkane (circle, N_2) vs molecule length.[77] (c) Transition from the tunneling regime to the hopping regime of (CG) DNA molecules inserted with (AT) tunneling blocks (blue triangle). (CG) sequence DNA molecules do not show transition behavior (black squares).[79] Reproduced with permission from Li *et al.*, Nat. Commun. **7**, 11294 (2016). Copyright 2016 Macmillan Publishers Ltd. (d) Experimental (square, left axis) and computational (circle, right axis) results of C_{60} monomer, dimer and trimer (only computational data shown for trimers).[80] Reprinted with permission from Evangeli *et al.*, Nano Lett. **13**, 2141 (2013). Copyright 2013 American Chemical Society.

maintained at a constant value using feedback control (Fig. 4(b)). The electrical conductance and the Seebeck coefficient of the tip-SAM-metal junctions are directly measured by monitoring the current output under a small bias and by measuring the voltage output under a temperature difference.

Mechanically controlled break junction (MCBJ) technique is another widely used experimental approach for probing the electrical and thermoelectric transport properties of MJs. The first mechanical "break junction" experiment was conducted by Moreland and Ekin[64] for electron tunneling in superconductors. Later Muller and van Ruitenbeek[65] developed a MCBJ technique in which a suspended metallic wire with a notch at the center is attached to a thin substrate (Fig. 4(c)). Further, the flexible device is mounted in a three-point contact configuration. The center of the device is pushed by a piezoactuator whose motion can be controlled precisely by external bias. This process results in an elongation of the wire and eventually leads to the fracture of the wire at the notch, exposing clean metal surfaces. By controlling the motion of the actuator, the gap size between the electrodes can be systematically controlled allowing one to close and reopen the gap. Specifically, the displacement between the electrodes is a small fraction (also called reduction factor) of the displacement of the actuator due to the geometry of the MCBJ platform. This reduction factor enables very precise control of the separation of the electrodes with picometer stability. Given the excellent stability of the MCBJ technique, it has been employed extensively in studies of transport properties of MJs and atomic junctions.[66–74]

Reed *et al.*[73] applied the MCBJ technique to perform charge transport measurements in organic molecule based MJs. Briefly, they exposed the Au electrodes in an MCBJ setup to benzenedithiol (BDT) molecules. This enabled them to successfully trap BDT molecules between the Au electrodes. Given the stability of the MCBJ platform, they were able to trap MJs and perform electrical transport experiments in them.

Tsutsui *et al.*[74] adapted the MCBJ technique for probing thermoelectric properties of MJs by integrating a Pt serpentine heater into one of the electrodes, which enabled them to apply temperature differentials across MJs (Fig. 4(c)). Using this approach, the authors probed both the electrical conductance and the Seebeck coefficient of Au–BDT–Au junctions and reported that the transport properties were sensitive to the geometric configuration of BDT molecules. They showed that upon mechanical stretching, in some cases, the molecule tilts into an upright direction and the Au–S bonds are elongated, resulting in a weaker coupling to the contact and a gradual shift of the HOMO level, accompanied by a decrease in conductance and a change (slight increase or decrease) in the Seebeck coefficient. In other cases they found that the configuration of the contact was dramatically changed, so that E_F shifted towards HOMO level, leading to an increased conductance and Seebeck coefficient.

2. Length dependence of thermopower in molecular junctions

Researchers have explored the dependence of the thermoelectric properties of MJs on molecular length. For Au–alkanedithiol (ADT)–Au junctions, the thermopower was found (Fig. 5(a)) to decrease linearly with increasing N (N is the number of carbon atoms in the backbone).[75] In contrast, for aromatic MJs, e.g., Au–phenylenediamine–Au[75] and Au–phenylenedithiol–Au[59,75,76] junctions, the thermopower was found to increase linearly with length (Fig. 5(a)). The authors[75] attributed the opposite trend in alkanedithiols to the presence of metal induced gap states. For aromatic junctions similar results were found by Widawsky *et al.*[77] for trimethylstannylmethyl-terminated polyphenyls with 1–4 phenyl rings (P1–P4) (Fig. 5(b)). However, they also found that the thermopower of trimethylstannyl-terminated alkanes with N = 6, 8, and 10 (C6, C8, and C10) has little length dependence (Fig. 5(b)).

Length dependence of thermopower was also studied in junctions made from DNA molecules of different sequences

(Fig. 5(c)).[78,79] For GC sequence double-stranded DNA molecules, Li *et al.*[79] reported a linear increase in resistance with molecular length whereas the Seebeck coefficient was small and weakly dependent on the length. This is because hopping of holes along the molecules dominates the charge transport in GC sequences where Gs act as hopping sites. When AT pairs, which are expected to act as a tunneling barrier, were inserted in the middle of GC sequence, both the conductance and thermopower changed. It was found that when the number of inserted AT block base pairs m is smaller than 4, the resistance increased exponentially with the length of the block, and the Seebeck coefficient increased linearly and is large compared with the size of the GC molecule. When $m \geq 4$, the transport mechanism was reported to transition from tunneling to hopping, in which regime the resistance shows weak dependence on length, and the Seebeck coefficient drops to small values.

In addition to the above described measurements of length dependence, Evangeli *et al.*[80] created a C_{60} dimer by contacting a tip that had one C_{60} molecule adhered to it with another C_{60} molecule which adhered to a Au substrate (Fig. 5(d)). They found that the thermopower of the C_{60} dimer is approximately doubled in comparison to single C_{60} junctions, resulting in a relatively high Seebeck coefficient of $-33\ \mu V/K$. Computational results suggested that the thermopower and ZT increased with the number of C_{60} monomers in the molecular chain due to the intermolecular interaction, suggesting that it may be possible to improve thermoelectric properties by manipulating C_{60} junctions.

3. Effect of end groups on thermoelectric properties

The end groups bridging molecules to electrodes play an important role in charge transport and thermoelectric properties of MJs.[81–84] Experimental measurements of thiol-terminated aromatic MJs showed a positive thermopower[34,74,75] while measurements of isocyanide-terminated junctions showed a negative thermopower.[85] In addition, experimental work on trimethyltin-terminated aromatic molecules[77] demonstrated slightly higher thermopower compared to thiol groups.[85] Balachandran *et al.*[83] provided a theoretical explanation for end-group effects on thermopower of MJs. Specifically, they investigated five different end groups (isocyanide, nitrile, amine, thiol, and hydroxyl) which couple triphenyl molecule to Au electrodes (Fig. 6) and studied the influence of end groups. They found that isocyanide, nitrile, and amine end-groups led to charge transfer out of the molecule upon coupling with the electrodes, resulting in a downward shift of the energy levels, which positioned the HOMO peak closer to the Fermi energy. In contrast, thiol and hydroxyl end-groups resulted in charge transfer from the electrodes into the molecule, which led to a slight downward shift in the energy levels thus placing the LUMO peak closer to the Fermi energy.

4. Effect of chemical structure, conformation and shape of molecules

The effect of chemical structure on thermoelectricity of MJs has been probed by adding electron-withdrawing/donating groups (fluorine, chlorine, and methyl) to BDT molecules (Fig. 7(a)).[86] It was suggested that the presence of electron-withdrawing groups (fluorine and chlorine) on a BDT molecule shifts the energy levels of MJs downwards, leading to a decreased thermopower, while the presence of electron-donating group (methyl) groups shift the energy levels upwards, leading to an increased thermopower. Since BDT has HOMO dominated charge transport properties, shifting the

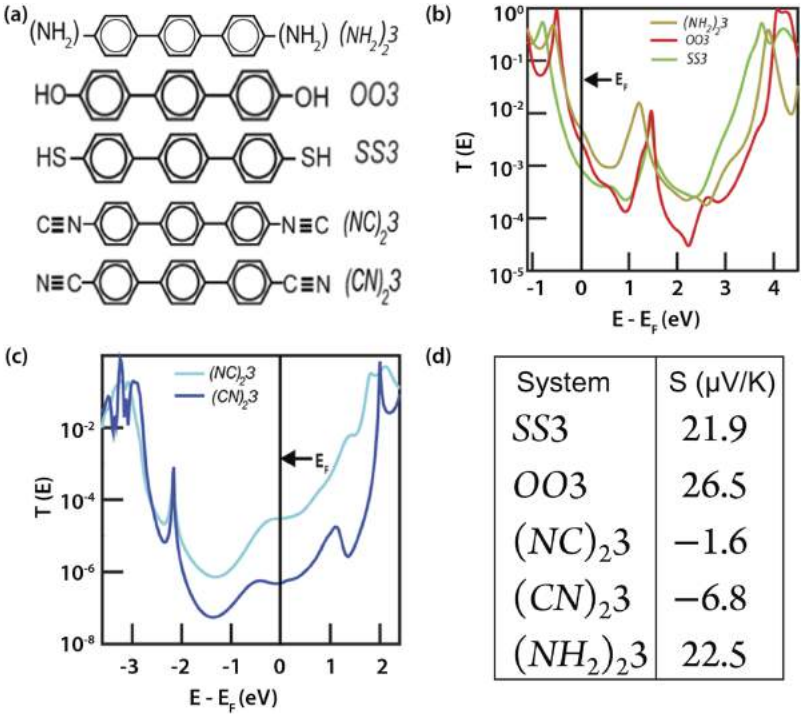

System	S (μV/K)
SS3	21.9
OO3	26.5
$(NC)_2 3$	−1.6
$(CN)_2 3$	−6.8
$(NH_2)_2 3$	22.5

FIG. 6. Theoretical results for triphenyl MJs with five different end groups.[83] (a) Schematic of triphenyl molecules with five different end groups. ((b) and (c)) Transmission as a function of energy. For SS3, OO3, and $(NH_2)_2 3$ molecules, the HOMO peak is closer to the E_F. For $(NC)_2 3$ and $(CN)_2 3$ the LUMO peak is closer to the E_F, resulting in a LUMO-dominated transport. Reproduced with permission from Balachandran *et al.*, J. Phys. Chem. Lett. **3**, 1962 (2012). Copyright 2012 American Chemical Society. (d) Calculated Seebeck coefficient for five types for triphenyl molecular junctions.

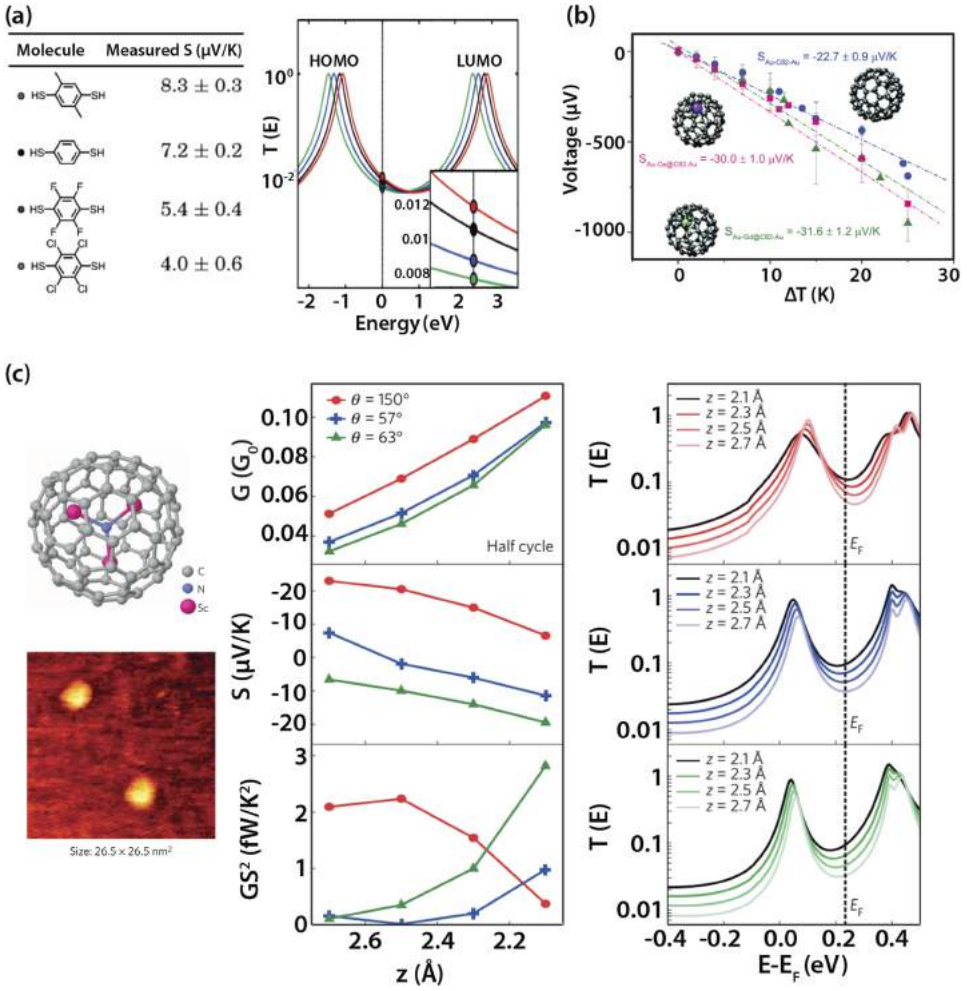

FIG. 7. Effect of chemical structure, conformation, and shape of molecules on thermoelectric properties of MJs. (a) Thermoelectric properties of BDT based MJs with substituents.[86] Left: Structure of BDT2Me, BDT, BDT4F, and BDT4Cl molecules (from top to bottom). Right: Lorentzian shaped transmission functions which illustrates how the transmission function is expected to change due to electron-withdrawing groups (BDT4F, blue line; BDT4Cl, green line; and BDT, black line) and electron-donating groups (BDT2Me, red line). Reproduced with permission from Baheti *et al.*, Nano Lett. **8**, 715 (2008). Copyright 2008 American Chemical Society. (b) Seebeck coefficient of C_{82} derivative based junctions: C_{82} (blue circle), Gd@C_{82} (green triangle), and Gd@C_{82} (magenta square).[90] Reproduced with permission from Lee *et al.*, Nanoscale **7**, 20497 (2015). Copyright 2015 Royal Society of Chemistry. (c) Effect of mechanical deformations of molecular junctions on their thermoelectric properties.[91] Left: Schematic of $Sc_3N@C_{80}$ molecule and two isolated $Sc_3N@C_{80}$ molecules under STM. Middle: Conductance, Seebeck coefficient, and power factor (GS^2) as functions of pressing distance. Red circle, blue square, and green triangle represent different molecule orientations corresponding to the substrate. Right: Theoretical transmission functions vs. energy. Red, green, and blue represent different molecular orientations. Lighter colored line represents larger pressing distances.[91] Reproduced with permission from Rincon-Garcia *et al.*, Nat. Mater. **15**, 289 (2016). Copyright 2016 Macmillan Publishers Ltd.

energy levels up (down) gives rise to a larger (smaller) slope in the transmission function at the Fermi level.

The effect of molecular conformation on the electrical conductance has also been studied by several groups.[87–89] For example, it was shown that in aromatic molecules, when the planes associated with each of phenyl rings are twisted from being "flat" ($\theta = 0°$, θ indicates the twist angle between two benzene plates) to being "perpendicular" ($\theta = 90°$), the conductance decreases by a factor of 30.[87] The thermoelectric properties of MJs created from fullerene based molecules were investigated by Lee *et al.*[90] They experimentally investigated three fullerene derivatives (C_{82}, Gd@C_{82}, and Ce@C_{82}) and found enhanced thermopower of Gd@C_{82} and Ce@C_{82} (Fig. 7(b)). Computational analysis of the same system suggested that this enhancement was due to the encapsulated metal atoms that induced changes in the geometric and electronic structure of the fullerene molecule.

Researchers have also explored the effect of mechanical deformations of MJs on their thermoelectric properties.[74,91] For example, by studying Au–$Sc_3N@C_{80}$–Au junctions, where an Sc_3N molecule is imbedded into a C_{80} cage (Fig. 7(c)), Rincon-Garcia *et al.*[91] found that the magnitude and the sign of thermopower both depend on the orientation of the molecule and force applied to the molecule. Further, computational analysis by the authors also suggested that the introduced Sc_3N creates a sharp resonance near the Fermi energy, and the location of the peak in transmission function depends strongly on the molecular orientation and applied pressure, so the thermopower can exhibit both a positive and a negative sign, depending on the relative position of the transmission peak with respect to the Fermi level. They emphasized that the transport resonance plays an import role in thermoelectric performance and that $Sc_3N@C_{80}$ can act as a bi-thermoelectric material.

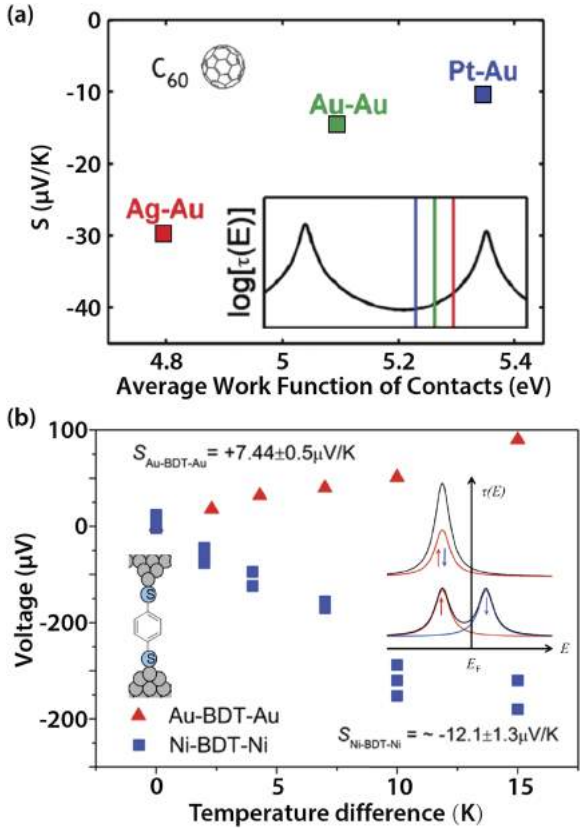

FIG. 8. Effect of electrode materials on thermoelectric properties of MJs. (a) Thermopower of Au–C_{60}–Au/Pt/Ag junctions vs. the average work function of electrodes. Inset: Lorentzian approximation of the transmission function, where blue, green, and red vertical lines approximate the position of E_F for Au–Pt, Au–Au, and Au–Ag junctions.[96] Reproduced with permission from Yee *et al.*, Nano Lett. **11**, 4089 (2011). Copyright 2011 American Chemical Society. (b) Plot of measured thermoelectric voltage of Au–BDT–Au (red triangle) and Ni–BDT–Ni (blue square) molecular junctions. Top inset: transmission function of Au–BDT–Au junction. Bottom inset: transmission function of Ni–BDT–Ni junction. Ni–BDT–Ni junction has a negative Seebeck coefficient (as opposed to the positive Seebeck coefficient of Au–BDT–Au junctions) due to spin-split hybridized states generated when BDT LUMO orbital coupled with Ni electrodes.[97] Reproduced with permission from Lee *et al.*, Nano Lett. **14**, 5276 (2014). Copyright 2014 American Chemical Society.

5. Effect of electrode materials

Although gold is the prototypical electrode material in most MJ experiments, other metals have also been studied to identify potentially interesting thermoelectric properties.[11,39,92,93] The advantage of other electrode materials lies in the possibility of bringing the Fermi energy of electrodes closer to the orbital that dominates the charge transport properties of molecules.[94,95] Past work on fullerene based molecules (C_{60}, PCBM ([6,6]-Phenyl-C_{61}-butyric acid methyl ester) and C_{70}) (Fig. 8(a), showing C_{60} only) showed that the Seebeck coefficient is suppressed when one of the Au electrodes is replaced by Pt. In contrast, it was found that the Seebeck coefficient is doubled when one of the Au electrodes was replaced with Ag.[96] Enhancements in the Seebeck coefficient were also reported in experiments involving Ni electrodes. Computations revealed that these enhancements arise from the spin-split hybridized states that are generated when the HOMO orbital of the BDT molecule couples with Ni electrodes (Fig. 8(b)).[97] In addition to these studies, computational work has pointed out that semiconducting electrodes[45] and carbon nanotubes[29] could suppress the "electron-like" contributions to the thermopower and cutoff the lower energy tails of HOMO transmission.[45] In these cases the output power of the systems was found to be greatly boosted.

6. Temperature dependence of thermopower in molecular junctions

According to Landauer formula, thermopower is expected to be linearly dependent on the average temperature of the molecular junction (see Eq. (2)). Kim *et al.*[98] varied the average temperature of Au–BDT–Au MJs and experimentally verified this prediction (Fig. 9). Since the figure of merit ZT is proportional to the power factor (G_eS^2) and temperature T, and inversely proportional to the thermal conductance G_{th}, this work indicates that ZT can potentially increase as T^3 if the thermal conductance is independent of temperature, as is expected when the operating temperature is higher the Debye temperature of the electrodes.

7. Three-terminal thermoelectric measurements

Key to improving the thermopower of a MJ is to modify the transmission function such that the slope and magnitude of the transmission function at the Fermi energy are maximized. However, most measurements of thermoelectric properties of MJs have relied on two-terminal measurements, which do not offer control on the electronic structure of the junction. Past research[99–109] has shown that it is possible to create three-terminal devices that can tune the electronic structure of junctions via a gate electrode. These devices are often created by a process called

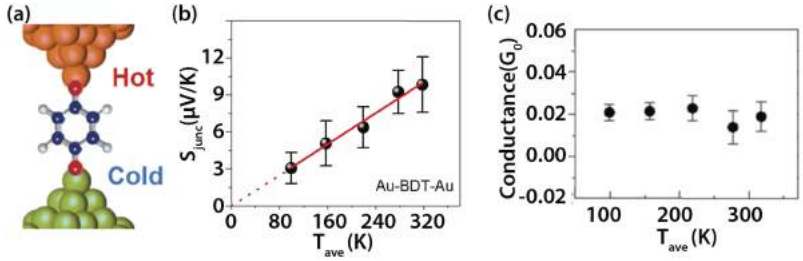

FIG. 9. Temperature dependence of thermopower of molecular junctions.[98] (a) Schematic of a Au–BDT–Au junction. (b) Plot of measured Seebeck coefficient as a function of average temperature of the junction. Linear fit indicates that the Seebeck coefficient vanishes when the temperature tends to 0 K. (c) Plot of the electrical conductance as function of average temperature. The electrical conductance remains invariant with temperature. Reproduced with permission from Y. Kim *et al.*, Appl. Phys. Lett. **109**, 033102 (2016). Copyright 2016 AIP Publishing.

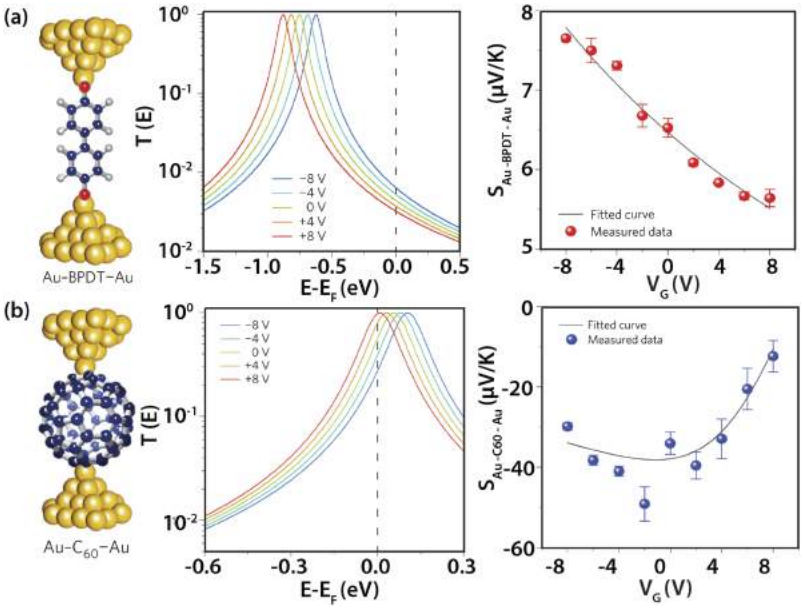

FIG. 10. Electrostatic tuning of thermoelectric properties of MJs, Au–DBDT–Au (a) and Au–C_{60}–Au (b) junctions using three-terminal EBJ technique. Left: molecular junction structures. Middle: Lorentzian curves that approximate the transmission function when the gate voltage is varied from −8 V to +8 V. Right: measured Seebeck coefficient as a function of gate voltage.[111] Reproduced with permission from Kim *et al.*, Nat. Nanotechnol. **9**, 881 (2014). Copyright 2014 Macmillan Publishers Ltd.

electromigration which creates three-terminal MJs by inserting molecules in nanometer-sized gaps formed during electromigration.[103,110] In creating these devices, a gold nanowire is first fabricated using electron-beam lithography on a doped Si layer which is coated with a thin dielectric layer. Subsequently, a large electric current is applied to the nanowire, causing the movement of metal atoms, which creates a nanometer or sub-nanometer sized gap in the nanowire. Molecules are deposited into the nanoscale gap by exposing the electrodes to molecules in a solution. The broken portions of the Au nanowire create two terminals (source and drain electrodes), while the Si back gate serves as a gate electrode. While several groups have used three terminal devices for tuning electrical transport, such devices could not be readily used for thermoelectric measurements due to the challenges in establishing temperature differences across the nano-gap between electrodes.

In order to overcome the limitations of two-terminal thermoelectric measurements, Kim *et al.*[111] created novel three-terminal devices based on EBJ and integrated an electric heater into one electrode (source or drain) that allowed them to apply temperature differences across MJs while electrostatically gating their electronic structure. Using such devices (Fig. 4(d)), they probed the thermoelectric properties of Au–biphenyldithiol (BPDT)–Au and Au–C_{60}–Au junctions. These measurements revealed that the thermoelectric properties can be significantly improved when the dominant transport orbital is located closely to Fermi energy. In analyzing these experimental results, the transmission function of the junctions was approximated by a Lorentzian function. For both Au–BPDT–Au junction (Fig. 10(a)) and Au–C_{60}–Au junctions (Fig. 10(b)), the thermoelectric properties were found to be tunable when a gate voltage was applied. This work demonstrated the feasibility of improving thermoelectric properties by tuning the electronic structure of MJs.

IV. THERMAL TRANSPORT IN MOLECULAR JUNCTIONS

In this section we provide a review of the studies of thermal transport in MJs and polymer chains. We begin by first describing the computational and theoretical work on thermal transport in MJs. Subsequently, we will describe the status of current experimental work and compare the results from experiments with those from computational predictions.

A. Heat conduction

1. Computational results

Thermal transport in macroscopic systems is well described by Fourier's law, $J = -\kappa\nabla T$, where J is the heat current density, κ is the thermal conductivity, and T is the absolute temperature. However, numerous computational studies have suggested that Fourier's law is inapplicable to modeling thermal transport in single molecule chains and junctions. Historically, this important characteristic was identified in the pioneering work of Fermi, Pasta, and Ulam (the FPU problem)[112] where they studied the dynamics of a 1D lattice chain of N monoatomic particles. They found that a small nonlinearity in the harmonic 1D chain can give rise to a surprising divergence in thermal conductivity. Specifically, they found that for a chain of N atoms, the thermal conductivity varies as $\kappa \propto N^{\alpha}, \alpha > 0$. More recently, several other groups have explored thermal transport in 1D-chains based on the FPU chain model.[113,114] Specifically, simulations performed using non-equilibrium molecular dynamics (NEMD) and equilibrium Green-Kubo methods confirmed that a divergence in thermal conductivity is to be expected for various configurations of the interatomic potential as well as for chains with a diatomic basis. Several of these studies reported that the value of the exponent (α) is ~0.4, suggesting that such divergences are a general feature of 1D chains.

Despite the early theoretical findings leading to important insights into thermal transport in 1D atomic chains, the originally considered systems were relatively simple and did not include the effects of electrodes and the coupling between the chains and the electrodes. In order to capture these additional effects, more realistic 1D structures such as MJs and atomic junctions have also been recently explored. For example, Segal *et al.*[115] studied thermal conduction through alkane chains bridging two thermal reservoirs. They derived a Landauer-like expression for heat flux from a generalized Langevin equation. By considering the phonon modes of a given molecule and the thermal reservoir, they calculated the thermal conductance and revealed interesting dependencies of the thermal conductance on the length and temperature of the junction (Figs. 11(a) and 11(b)). Specifically, they found that in the presence of weak reservoir-molecule coupling, the molecule chain achieved a maximum thermal conductance when the number (N) of the back-bone carbon atoms equals 4. Further, they found that a size-independent conductance is established when $N > 10$, indicating a strong divergence in the thermal conductivity. However, they found that when the reservoir-molecule coupling was strengthened, a Fourier-like thermal conductivity was recovered.

Ab initio methods were also employed by Sadeghi *et al.*[116] to study the thermal conductance of alkanes (N = 2, 4, 8, and 16) and oligoynes (N = 2, 4, 8). They identified the contributions to the thermal conductance from electrons and phonons and found that the phononic contribution for alkanes is ~700 times larger than the electronic contribution. Similar calculations for oligoynes suggested that the phononic contribution is only 30 times larger than the electronic contribution. Further, similar to the findings of Segal *et al.*,[115] the thermal conductance of both alkanes and oligoynes in this work was found to first increase and then decrease with the molecule length (Figs. 11(c) and 11(d)).

More recently, Klöckner *et al.*[117] combined DFT and NEGF approaches to calculate the thermal conductance of alkanes (N = 2 to 30) and PTFE molecule (where H atoms in alkanes are replaced by F atoms) with different end anchoring groups (thiol and amine) (Figs. 11(e) and 11(f)). They reported that the phononic thermal conductances in all scenarios are relatively insensitive to the molecular length. Further, they explored the effect of the anchoring group by calculating the thermal conductance for both thiol- (–SH) and amine– ($–NH_2$) terminated MJs. They found that the thiol-terminated MJs had a higher conductance than the amine-terminated ones.

Markussen[118] performed first-principle simulations of phonon transport through both linear-conjugated and cross-conjugated molecules. He showed that in cross-conjugated molecules, such as meta-connected benzene, the phonon transmission function exhibits destructive quantum interference. This observation is analogous to the destructive quantum

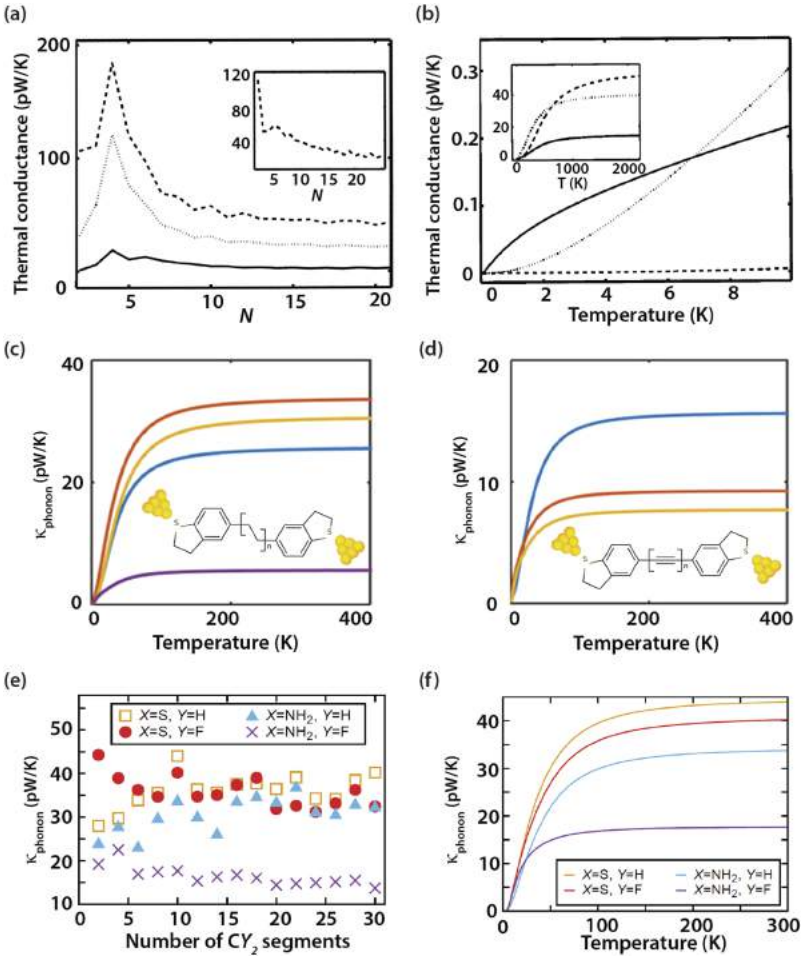

FIG. 11. Calculated thermal conductance of single molecule junctions. (a) Thermal conductance of alkane molecules vs. the chain length at different temperatures (solid line 50 K, dotted line 300 K, dashed line 1000 K) for the case of weak molecule-reservoir coupling.[115] Inset: calculations for the case of strong molecule-reservoir coupling at 1000 K. (b) Temperature dependent thermal conductance of alkane molecules for different chain lengths (number of carbon-atom in the back-bone N) (dashed line $N = 2$, dotted line $N = 5$, full line $N = 14$).[115] (a) and (b) reproduced with permission from D. Segal *et al.*, J. Chem. Phys. **119**, 6840 (2003). Copyright 2003 AIP Publishing. (c) Temperature dependent phononic thermal conductance of alkanes (chemical structure shown as inset, blue line n = 1, red line n = 2, yellow line n = 4, purple line n = 8).[116] (d) Temperature dependent phononic thermal conductance of oligoynes (blue line n = 1, red line n = 2, yellow line n = 4).[116] (c) and (d) reproduced with permission from H. Sadeghi, S. Sangtarash, and C. J. Lambert, Nano Lett. **15**, 7467 (2015). Copyright 2015 American Chemical Society. (e) Room temperature (300 K) phononic thermal conductance vs. number of CY_2 units (Y = H, F) in the molecule for different end anchoring groups X (X = S, NH_2).[117,175] (f) Temperature dependent phononic thermal conductance for molecules with 10 CY_2 units.[117,175] (e) and (f) reproduced with permission from Klockner *et al.*, Phys. Rev. B **94**, 205425 (2016). Copyright 2016 American Physical Society.

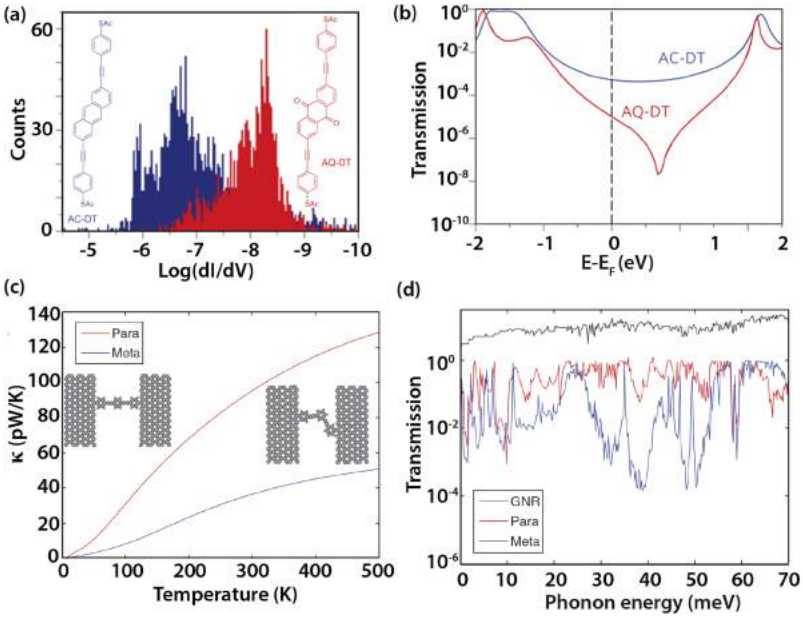

FIG. 12. Influence of quantum interference on electrical and thermal (phonon) transport. (a) Measured electrical conductance histogram of AC-DT and AQ-DT molecules (chemical structures shown as inset).[119] (b) Calculated transmission functions for AC-DT and AQ-DT.[119] Cross-conjugated AQ-DT molecule exhibits destructive electron interference effect. (a) and (b) reproduced with permission from Guedon *et al.*, Nat. Nanotechnol. **7**, 304 (2012). Copyright 2012 Macmillan Publishers Ltd. (c) Calculated phononic thermal conductance for para- and meta-connected molecules (chemical structures shown as insets).[118] (d) Calculated phonon transmission functions showing phononic quantum interference effect.[118] (c) and (d) reproduced with permission from T. Markussen, J. Chem. Phys. **139**, 244101 (2013). Copyright 2013 AIP Publishing.

interference effects for electron transport in similar molecules (Figs. 12(a) and 12(b)).[119] Further, he found that the cross-conjugated MJs reduce the thermal conductance by a factor of 2-5 compared to the linear-conjugated counterparts (Figs. 12(c) and 12(d)).

In addition to studies in single MJs, heat conduction through self-assembled monolayer (SAM) of molecules covalently bonded to the substrates has also been extensively investigated. Select computational results for different combinations of solid-SAM-solid/liquid junctions are summarized in Fig. 13. Specifically, Luo and Lloyd[120–122] performed non-equilibrium and equilibrium molecular dynamics (NEMD) calculations in Au–SAM–Au junctions. The thermal conductance of such junctions was found to be independent of length and the applied external pressure. These results were also confirmed by Duda *et al.*[123] who calculated the interface thermal conductance across the Au–SAM junctions. They found that the thermal conductance is nearly constant upon varying the molecular length. Further, Goicochea *et al.*[124] studied thermal transport across silica-SAM-water junctions. They found that compared to the silica-water junctions, the thermal conductance is enhanced by 1.8–3.2 fold when the silica surface is chemically functionalized by alkysilanol ($-Si(OH)_2-(CH_2)_n-OH$) to become hydrophilic. In addition, Hu *et al.*[125] studied thermal transport in Au–SAM–Si junctions using molecular dynamics simulations and found that the phonon

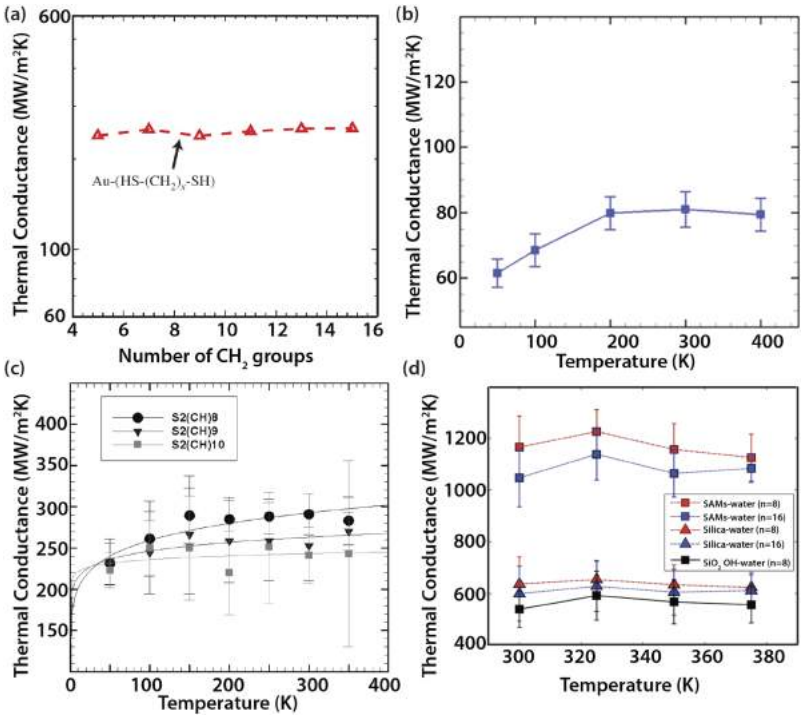

FIG. 13. Calculated thermal conductance of self-assembled monolayer (SAM) MJs. (a) Thermal conductance across Au–ADT monolayer interface vs. the number of CH_2 groups in the backbone.[123] Reproduced with permission from J. C. Duda *et al.*, J. Chem. Phys. **134**, 094704 (2011). Copyright 2011 AIP Publishing. (b) Temperature dependent thermal conductance of GaAs-ADT ($N = 8$)–GaAs MJs.[121] Reproduced with permission from T. F. Luo and J. R. Lloyd, J. Appl. Phys. **109**, 034301 (2011). Copyright 2011 AIP Publishing. (c) Temperature dependence of the thermal conductance of Au–ADT ($N = 8, 9, 10$)–Au junctions.[122] Reproduced with permission from T. F. Luo and J. R. Lloyd, J. Heat Transfer **132**, 032401 (2010). Copyright 2010 American Society of Mechanical Engineers. (d) Temperature dependence of the thermal conductance of SiO_2–SAM–water junctions.[124] The SAM MJs are formed by alkysilanol ($-Si(OH)_2-(CH_2)_n-OH$, $n = 8, 16$). Reproduced with permission from Goicochea *et al.*, J. Heat Transfer **133**, 082401 (2011). Copyright 2011 American Society of Mechanical Engineers.

transmission function shows distinct oscillatory behavior with strong frequency dependence, which indicates phonon interference effects. Further, they showed that this interference effect diminishes with increasing SAM thickness.

The observation of unusual phonon transport phenomena in MJs have led to several proposals for control and manipulation of thermal properties.[126] As shown in Fig. 14, it has been proposed theoretically that MJs can be used to create thermal rectifiers[127–130] (heat flow enhanced in one direction but suppressed in the other direction due to the asymmetrical molecule-reservoir coupling), field-effect phononic thermal transistors[131] (by reversibly switching between the acoustic torsion and optical phonon modes), mechanically tunable thermal modulators,[132] heat pumps[133] (flowing heat flux in the absence of temperature difference due to the phononic analogy of berry-phase effect), and quantum heat ratchets[134] (directed flow of current even when the net average temperature difference across the junction $\Delta T = 0$).

In addition to the studies of thermal transport in short MJs ($N < 30$), another interesting topic is thermal transport in long polymer molecular chains. Here, computational/theoretical work was mainly inspired by the experimental observation[135] of high thermal conductivity in highly drawn polyethylene (PE) fibers. In contrast to the explorations of thermal transport in 1D chains, long polymer molecules represent realistic 1D systems that can test the limit of Fourier's law. Many

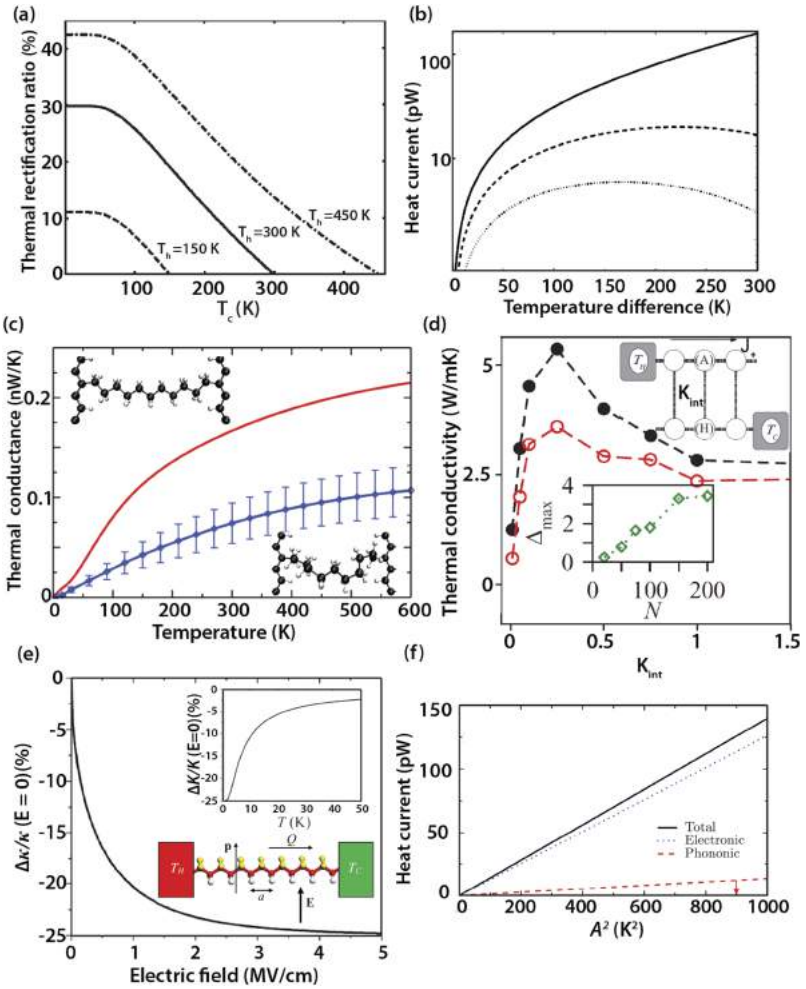

FIG. 14. Proposed schemes for controlling/modulating thermal transport. (a) Heat rectification ratio in a two-level phonon model as a function of T_c (cold reservoir temperature) when hot reservoir temperature T_h is fixed (dashed line 150 K, full line 300 K, dashed-dotted line 450 K).[128] Reproduced with permission from D. Segal and A. Nitzan, J. Chem. Phys. **122**, 194704 (2005). Copyright 2005 AIP Publishing. (b) Predicted negative differential thermal conductance (NDTC) in a two-level phonon model vs. temperature difference across the MJ.[129] The molecule-reservoir coupling strength is set to be weak (solid line), medium (dashed line), and strong (dotted line). Reproduced with permission from D. Segal, Phys. Rev. B **73**, 205415 (2006). Copyright 2006 American Physical Society. (c) Tunable thermal conductance in a MJ by mechanical compression/stretching.[132] Reproduced with permission from Li *et al.*, J. Phys. Chem. C **119**, 24636 (2015). Copyright 2015 American Chemical Society. (d) Heat rectification realized in a two-chain molecule model. Rectification ratio is plotted as a function of the interaction strength between the two chains.[130] One chain (labeled as H in the inset) has only harmonic interactions and the other (A) contains local nonlinearities. Inset shows the molecular length dependent rectification ratio. Reproduced with permission from E. Diaz, R. Gutierrez, and G. Cuniberti, Phys. Rev. B **84**, 144302 (2011). Copyright 2011 American Physical Society. (e) Modulated thermal conductance by applying electric field to tune the dipole moments of the monomers.[131] Inset shows the modulation ratio vs. temperatures. Reproduced with permission from Menezes *et al.*, Phys. Rev. B **81**, 012302 (2010). Copyright 2010 American Physical Society. (f) Heat ratchet effect in MJs. Predicted heat current (total and the separate electronic and phononic contributions) is plotted as a function of the square of the amplitude (A) of temperature oscillation.[134] The two reservoirs are at temperatures $T_L = T_0 + A\cos(\omega t)$, $T_R = T_0$. The driving frequency is $\omega = 3.92$ GHz, and $T_0 = 300$ K. Reproduced with permission from Zhan *et al.*, Phys. Rev. E **80**, 061115 (2009). Copyright 2009 American Physical Society.

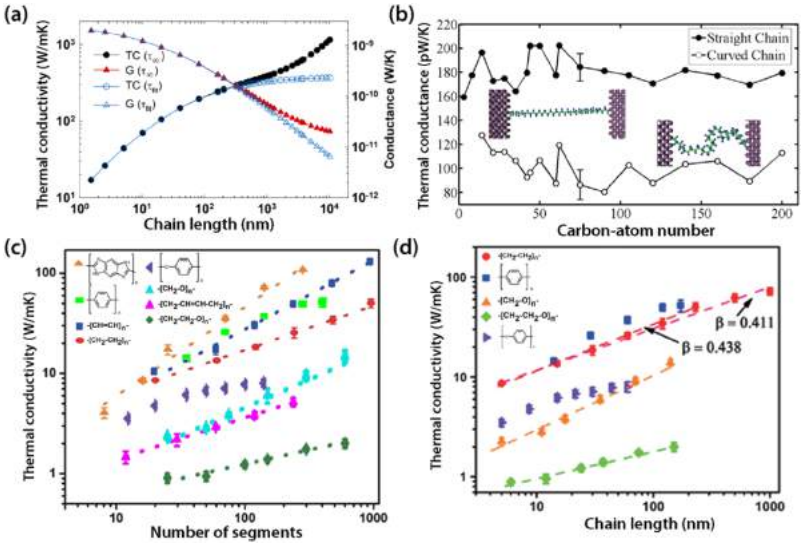

FIG. 15. Calculated thermal conductance of single polymer molecular chains. (a) Length dependence of thermal conductivity (circles) and corresponding conductance (triangles) for a single polyethelene (PE) chain.[21] Reproduced with permission from A. Henry and G. Chen, Phys. Rev. Lett. **101**, 235502 (2008). Copyright 2008 American Physical Society. (b) Length dependent thermal conductance of straight (solid circle) and kinked chains (open circles).[138] The ratio of end-to-end distance to contour length is 0.55 for the kinked chains. Reproduced with permission from K. Sasikumar and P. Keblinski, J. Appl. Phys. **109**, 114307 (2011). Copyright 2011 AIP Publishing. (c) Thermal conductivity of single chains of various polymers vs. the number of segments.[22] (d) Length dependent thermal conductivity of various types of polymer chains.[22] (c) and (d) reproduced with permission from J. Liu and R. G. Yang, Phys. Rev. B **86**, 104307 (2012). Copyright 2012 American Physical Society.

researchers[21,22,136–138] have simulated thermal conduction in single polymer chains of various lengths and found that the thermal conductivity is several orders of magnitude higher than that in bulk materials. Similar to the results from the simple 1D lattice model, thermal conductivity increases with molecular length, and even shows divergence in some cases. Particularly, Henry and Chen found that the thermal conductivity of a single PE chain can reach 350 (W/m)/K when the molecular length is longer than 1 μm (Fig. 15(a)).[21] Further, Sasikumar and Keblinski[138] studied the role of chain conformation on phonon transport. They found that by introducing gauche conformations (kinks), the curved chain was shown to have much smaller thermal conductance than the straight chain because of the increase of phonon scattering centers (Fig. 15(b)). Further, Liu and Yang[22] found that the polymer chains with aromatic monomers had a thermal conductivity ~5 times larger than that of a PE chain (Figs. 15(c) and 15(d)) and concluded that thermal transport in these long molecular chains was determined by the competition between ballistic and diffusive phonons.

Another topic of interest in the study of thermal transport in molecular junctions and chains is the development of strategies to suppress phononic thermal conductance. Such strategies can positively affect thermoelectric energy conversion efficiency of molecular devices by reducing phononic thermal conductance. Proposals in this direction include, for example, taking advantage of the degree of mismatch in the vibrational (phonon) density of states of the electrodes (which is effectively continuous) and the molecules (which are discrete)[116,139] as well as designing π-stacked molecular structures with weak coupling between different parts of the molecules.[140]

2. Experiments

While computational studies of thermal transport have been pursued for several years, corresponding experimental investigations have begun only recently. The strategy to quantify molecular thermal conductance is conceptually straightforward. An applied temperature difference (analogous to a voltage bias applied during electrical measurements) results in a relatively small heat current (analogous to electrical current) across the MJs, which need to be measured to quantify thermal conductances. Given the challenges associated with measuring the small heat currents in that arise in MJs (especially single molecule junctions), experimental studies have been somewhat limited.

The primary platform employed for probing thermal transport in MJs are SAM based junctions as they provide a well characterized junction structure with a relatively large area over which experiments can be performed.[141] Some of the first transport studies were performed across solid-SAM-liquid junctions. For example, Ge *et al.*[142] studied the thermal conductance in solid-SAM-water junctions. In this experiment the SAM (OTS, C_{18}, PEG-silane, $C_{11}OH$) was bonded to a solid surface (Au or Al) to chemically modify the surface. The measurement of thermal conductance of the junction was performed using the time domain thermoreflectance[143] (TDTR) technique, which characterizes the thermal conductivity of a thin film by measuring the temperature-dependent change of surface reflectance under transient laser heating. They found that the thermal conductance between hydrophilic surfaces and water was several times larger than that between hydrophobic surfaces and water, indicating the important role of the SAM on modulating the interface thermal transport. These findings were also confirmed by Tian *et al.*[144] who studied the thermal transport across the solid-liquid interface. They found that by adding a SAM (thiolated alkane molecules) between Au and ethanol the thermal conductance is enhanced 2-5 times, depending on the length of the MJs.

In addition to the studies of Solid-SAM-liquid configuration, MJs have also been studied in solid-SAM-solid configurations. Specifically, Wang *et al.*[139] measured the thermal conductance of Au–ADT–GaAs junctions (N = 8, 9 and 10). The molecular junction sample was prepared by a nanotransfer printing technique, where a gold thin film, patterned on a silicon stamp, was transferred onto a SAM chemically bonded to a GaAs substrate. Subsequently, the patterned Au film was employed as a thermometer to measure the thermal conductivity of the SAM junctions using the 3ω method.[145] In this work,

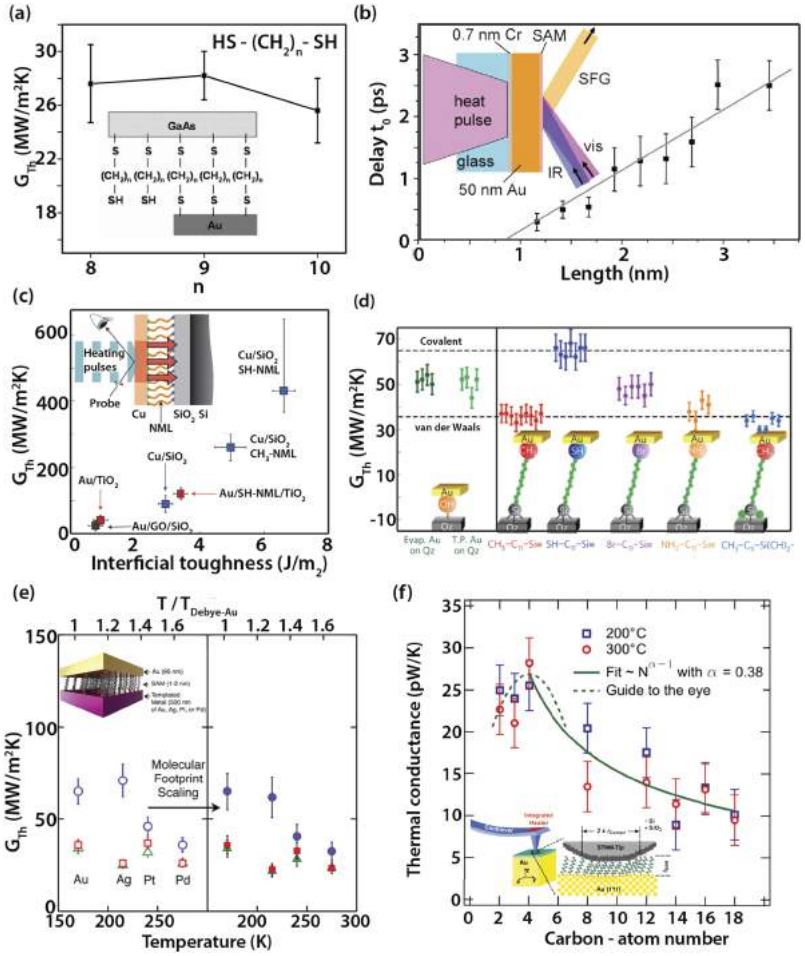

FIG. 16. Measured thermal transport in SAM based MJs. (a) Thermal conductance of Au–alkanedithol (n = 8, 9, 10)–GaAs junctions at room temperature.[139] Inset: schematic of the sample. Reproduced with permission from R. Y. Wang *et al.*, Appl. Phys. Lett. **89**, 173113 (2006). Copyright 2006 AIP Publishing. (b) Thermal conductance measurement on Au–alkanethiol ($HS–(CH_2)_n–CH_3$, n = 5 to 23) junctions.[42] The delay time between the heating laser pulse and the arrival of heat burst at the methyl head group is plotted as a function of the molecular length. Inset: schematic of the experimental set-up. Reproduced with permission from Z. H. Wang *et al.*, Science **317**, 787 (2007). Copyright 2007 AAAS. (c) Thermal conductance in metal-SAM-dielectric junctions obtained using the TDTR technique (schematics shown as inset).[146] Reproduced with permission from O'Brien *et al.*, Nat. Mater. **12**, 118 (2013). Copyright 2013 Macmillan Publishers Ltd. (d) Measured thermal conductance of SAM junctions for various end-groups.[147] Reproduced with permission from Losego *et al.*, Nat. Mater. **11**, 502 (2012). Copyright 2012 Macmillan Publishers Ltd. (e) Quantification of impact of vibration mismatch on thermal conductance.[148] The vibrational mismatch is introduced by using different metallic electrodes (with different Debye temperatures, i.e., cutoff phonon mode frequencies). The raw data (left half panel) were re-scaled by the molecular footprint to isolate the effect of the electrode vibrational spectra on thermal conductance (right half panel). Reproduced with permission from Majumdar *et al.*, Nano Lett. **15**, 2985 (2015). Copyright 2015 American Chemical Society. (f) Length dependent thermal conductance in Au–alkanethiol-SiO_2 junctions by scanning thermal microscopy (SThM) technique.[150] Reproduced with permission from Meier *et al.*, Phys. Rev. Lett. **113**, 060801 (2014). Copyright 2014 American Physical Society.

the measured thermal conductance was found to be insensitive to the length of the MJs (Fig. 16(a)).

In another work, Wang *et al.*[42] studied thermal transport through long-chain alkanethiols of various lengths that were bonded to a Au substrate (Fig. 16(b)). A nonlinear coherent vibrational spectroscopy technique, called the time-resolved sum-frequency generation (SFG) technique, was employed to detect the ultrafast thermal induced orientational disorder when heat is transported to the terminal $–CH_3$ head groups. They found that phonon transport in the alkane chains is ballistic and the thermal conductance, which is estimated to be ~50 (pW/K)/molecule, is limited by the Au–SAM interface.

These original experiments of thermal transport in solid-SAM-solid junctions not only demonstrated how thermal transport could be systematically probed but also identified several questions that needed further elucidation; for example, what is the influence of the SAM's molecular structure, the chemical composition of the electrodes, and the interactions between the molecule and the electrode on their thermal transport properties? How can the geometry of MJs be controlled to optimize (maximize or minimize) the thermal conductance? Several studies have been performed to answer these questions and are described below briefly.

O'Brien *et al.*[146] probed the thermal conductance of metal-SAM-dielectric interfaces and compared them to the thermal conductance of metal-dielectric interfaces. The samples were prepared by assembling different organosilane molecules with identical molecular structure except for the end groups (one with –SH, another with $–CH_3$) on two different dielectric structures (SiO_2 or TiO_2). By employing the TDTR technique, they demonstrated that the thermal conductance across the interfaces can be significantly increased (more than

a factor of 4) by introducing strong bonding organic monolayers to facilitate phonon transport through both metal-molecule and dielectric-molecule interfaces (Fig. 16(c)). Specifically, they found that the –SH end-group functionalization is more effective in boosting thermal transport than the $–CH_3$ end-group functionalization and demonstrated that interfacial thermal conductance can be tuned over an order of magnitude by altering the interfacial bonding strength.

In addition to the study of O'Brien *et al.*, Losego *et al.*[147] systematically measured the thermal conductance of Au–SAM-quartz junctions. All the organic molecules studied had a silane group ($–SiH_3$) at one end, while the other end was varied to be methyl ($–CH_3$), thiol (–SH), amine ($–NH_2$), or bromine (–Br). Their measurements of thermal transport revealed that the binding strength had a strong impact on the conductance. Specifically, they found that covalent-like bonds at the interface such as thiol-gold bonds yielded a thermal conductance that was ∼2 times higher than that given by van der Waals interactions, such as the cases with a $–CH_3$ moiety (Fig. 16(d)) interacting with Au. Further, they observed a linear dependence of interfacial thermal conductance on the covalent bond density, suggesting that intermolecular interactions do not significantly contribute to thermal transport.

More recently, Majumdar *et al.*[148] studied the impact of vibrational mismatch of electrodes on the thermal transport characteristics of SAM junctions. This measurement was conducted by employing a frequency-domain thermoreflectance[149] (FDTR) technique. Different from the TDTR technique, which records the time domain response of the surface reflectance due to temperature change, the FDTR technique records the frequency domain response. They found that Au–ADT–Au junctions yield a thermal conductance that is ∼2 times higher than Au–ADT–Pd junctions (Fig. 16(e)). The ratio of the Debye temperatures of the electrodes that sandwich the MJs was used as a measure of the vibrational mismatch between the electrodes to explain the differences in the thermal conductance. These studies show that since thermal transport in MJs is dominated by phonons, the vibrational modes inside the electrodes matter significantly even though the thermal carriers inside the electrodes are electrons.

In addition to the above conclusions, Meier *et al.*[150] performed experiments where they probed thermal transport using scanning probes with integrated heater thermometers in a vacuum environment. Their measurements were performed on SAM layers assembled between a Au surface and a silica-coated tip of their scanning probe. Specifically, they created Au–ADT–SiO_2 junctions, where one end group (–SH) was chemically bonded to the Au substrate while the other ($–CH_3$) was weakly interacting with the tip and studied heat flow from a heated substrate into their tip as the length of the molecules was varied. They found that the thermal conductance of Au–ADT–SiO_2 junctions showed a maxima when the number of carbon atoms (N) was increased from 2 to 4. Upon further increasing N from 8 to 14, the thermal conductance was found to be invariant within measurement uncertainty (Fig. 16(f)). This observed length-dependent thermal conductance matched well with the predictions by Segal *et al.*[115] We note that the advantage of the SThM over the former techniques is the capability to probe thermal transport in a highly localized region (<10 nm).

To summarize, current experimental work has successfully examined thermal transport properties of MJs in monolayers. However, experimental elucidation of thermal transport in single molecule junctions and single polymer chains has remained inaccessible. Specifically, the prediction of ultrahigh thermal conductivity in single polymer chains remains unverified. However, noteworthy efforts have succeeded in probing the thermal conductivity of nanofibers of polymer materials.[151–153] Such polymer nanofibers, which contain thousands or more single polymer chains, have provided an interesting preview of the thermal transport phenomena that arise in single-polymer chain based predictions. However, directly connecting the results from such nanofiber measurements to those of single polymer chains is complicated due to an incomplete knowledge of the crystallinity, orientation of the polymer fibers and the cross-linking between the chains.

B. Heat dissipation, local heating and cooling

Electric current flow and heat dissipation are often concomitant and involve complicated interactions among energy carriers. When a current I is driven by a constant bias V applied across a nanoscale junction, the total power dissipation is $Q = IV$. In MJs created from short molecules, if the transport through the molecular region is elastic, the Landauer approach can be used to describe heat dissipation at the electrodes of the MJs as described by Eqs. (5) and (6).

Inelastic processes, such as those arising from electron-phonon interactions in the molecular region pose significant challenges to modeling and result in a fraction of the power being dissipated in the molecular region. Given the small heat capacity of the molecules, even a small amount of heat dissipation leads to a significant increase in the local kinetic energy of atoms in the molecular region. Such scenarios raise important questions regarding the validity of the notion of temperature in this strongly non-equilibrium state. It is well known that the classical definition of temperature is applicable to only systems in equilibrium and is given by $T = \frac{\partial U}{\partial S}$, where U is the internal energy of the system and S is its entropy. Therefore, the description of non-equilibrium scenarios that arise during dissipation requires the definition of an operational temperature (also called the "effective temperature"[11]). Below, we provide a description of the computational and experimental work that was performed to understand heat dissipation in MJs.

1. Computational results

Various computational works have investigated heat dissipation and local heating effects in MJs and the microscopic mechanisms behind these phenomena. For example, heat dissipation in MJs was studied by Zotti *et al.*[38] based on the Landauer picture (Fig. 17). They performed *ab initio* transport calculations and showed that heat dissipation in short molecular junctions, where transport is expected to be elastic, is intimately related to the electronic structure of MJs. Specifically, they found that the heat dissipated in the two electrodes

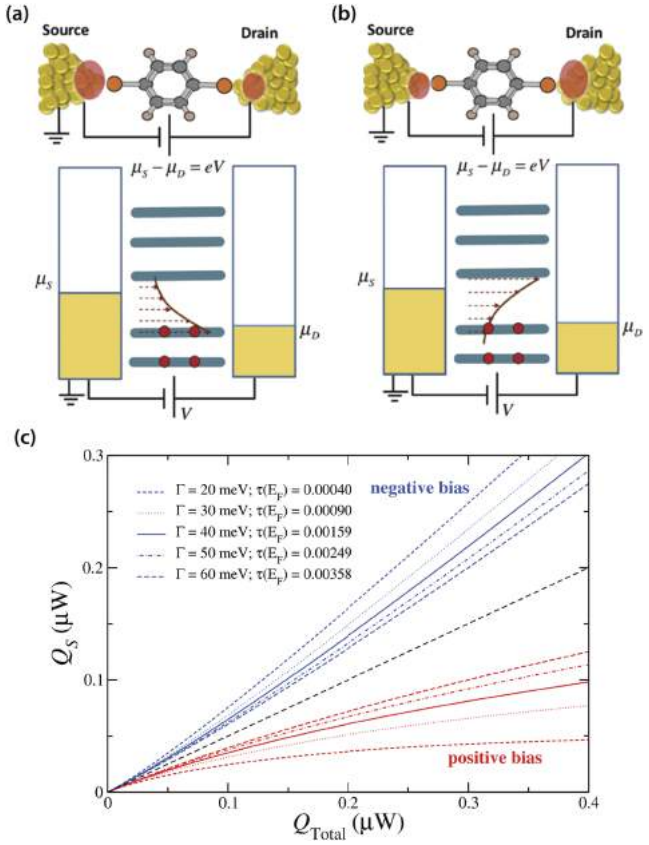

FIG. 17. Heat dissipation in MJs and the calculated heat dissipation based on the Laudauer model.[38] (a) Schematic describing asymmetric heat dissipation in the electrodes of a MJ. The potential drop across the left electrode-molecule interface is more than that across the right one. (b) Schematic of asymmetric heat dissipation in a MJ where the voltage drop is larger at the interface with the right electrode. The potential drop across the right interface is more in this case. (c) Calculated heat dissipation asymmetry for different molecule-electrode coupling strengths. Q_{Total} is the total heat dissipation and Q_S is the heat dissipated in the source electrode. Reproduced with permission from Zotti *et al.*, New J. Phys. **16**, 015004 (2014). Copyright 2014 IOP Publishing.

of a MJ is in general asymmetric and the degree of asymmetry is determined by the sign and magnitude of the thermopower of the MJs.

Heat dissipation in systems featuring inelastic effects (non-Landauer picture, Fig. 18(a)) was studied by Segal and Nitzan[154] where they estimated the fraction of heat dissipated in the molecular region and its dependence on the molecular length and coupling strength of the molecule with the electrodes. By comparing the predictions from different models (Fig. 18(b)), they found that the classical heat conduction theory underestimates the temperature rise in the molecular region, suggesting the need to apply microscopic models to understand the phonon energy transport in MJs.

Based on first principle approaches, Pecchia *et al.*[155] presented a theory of heat dissipation and local temperature of MJs. They found that local temperature is strongly influenced by electron-phonon scattering. By applying this theory to metal-styrene–Si junctions, they found that the local temperature sharply increases after a critical bias, which indicates the strong excitation of the lowest vibrational mode in the styrene molecules. Along these lines, Galperin *et al.*[156] also studied heating in current-carrying MJs and obtained a unified model to describe both heat dissipation and the electronic and vibrational contributions to heat conduction in MJs.

In addition to the contribution of electron-phonon scatterings to local heating, the effect of electron-electron scatterings has also been studied by D'Agosta *et al.*[157] who derived a model to describe the local temperature based on an electron liquid based hydrodynamic approach. They found that in MJs the electron-electron interactions, which could have comparable scattering rate as the electron-phonon interactions, may play an important role in determining the local temperature.

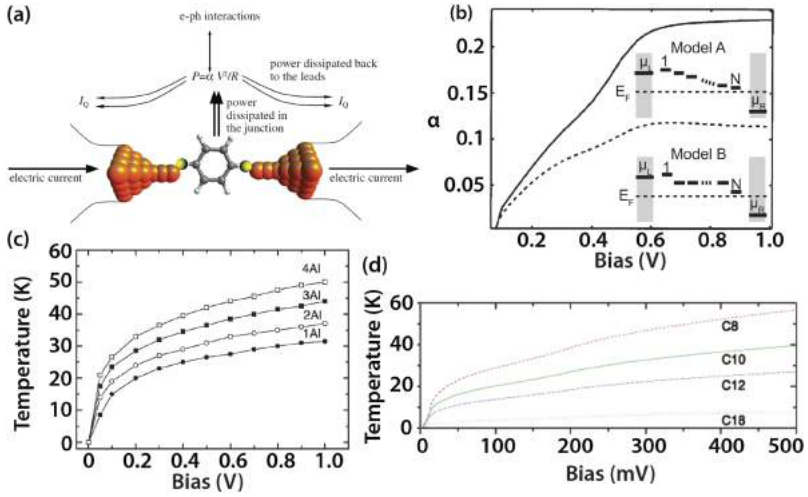

FIG. 18. Computational results on heat dissipation and local temperature in molecular junctions. (a) Schematic of heat dissipation in molecular junction due to inelastic scattering.[11] The total heat dissipation is V^2/R, of which $\alpha V^2/R$ is dissipated in the molecular region while the rest in the electrodes. Reproduced with permission from Y. Dubi and M. Di Ventra, Rev. Mod. Phys. **83**, 131 (2011). Copyright 2011 American Physical Society. (b) Predicted heat dissipation in molecular region (α) based on different models of potential distribution within the junction.[154] Reproduced with permission from D. Segal and A. Nitzan, J. Chem. Phys. **117**, 3915 (2002). Copyright 2002 AIP Publishing. (c) Local temperature increase calculated for atomic chains (with 1 to 4 Al atoms) under different biases.[158] Reproduced with permission from Yang *et al.*, Phys. Rev. B **71**, 041402 (2005). Copyright 2005 American Physical Society. (d) Local temperature increase as a function of bias voltage using alkanethiols of various lengths.[159] Reproduced with permission from Y. C. Chen, M. Zwolak, and M. Di Ventra, Nano Lett. **5**, 621 (2005). Copyright 2005 American Chemical Society.

The effect of molecular length on local heating was also studied by Yang *et al.*[158] who calculated the local temperature increase in MJs containing 1 to 4 Al atoms. Specifically, they found that at a given bias the local temperature increase is larger in longer chains (Fig. 18(c)). Further, Chen *et al.*[159] estimated the local heating of various ADT MJs (Fig. 18(d)). They found that in the presence of good molecule-electrode coupling, the local temperature increase was smaller when the molecular length increases. Further, local temperature increase was predicted to be insensitive to the molecular length when the molecule-electrode coupling was weak. These works suggest that inelastic interactions inside the molecule and heat dissipation in the electrodes play important roles in determining the local temperature.

In addition to studies of local heating effects, local cooling in MJs has also attracted much attention.[160–164] For example, Galperin *et al.*[160] proposed two cooling mechanisms: one based on the depletion of hot electrons inside the high potential electrode; the other based on inelastic electron transport. The former achieved a cooling effect by shifting the non-equilibrium electron distribution, which defines the effective temperature. The latter leveraged the inelastic tunneling in which the electron extracts energy from vibrational modes while transmitting through the junction. More recently, Lykkebo *et al.*[164] studied local cooling effects in realistic MJs. They presented cooling schemes based on inelastic electron tunneling and found that under voltage biases across the MJs the local temperature can potentially reach values below the ambient temperature. This study pointed out the possibility of realizing local molecular cooling by rationally designing the MJs.

2. Experiments

Several experimental studies have been performed to quantify heat dissipation in MJs and obtain insights into the inelastic processes in the molecular region and the electrodes. One of the first studies in this area was conducted by Huang *et al.*[165] who studied current induced local heating in MJs by measuring the force required to break the molecule-electrode covalent bonds. By taking advantage of the fact that the chemical bond breakdown process is thermally activated, the authors were able to define an effective temperature of the junction as a function of the applied bias. Based on their analysis they suggested that, under ambient conditions, an ~30 K temperature increase is generated when a bias of 1 V is applied across Au–octanedithol–Au junctions (Fig. 19(a)).

The instability of MJs induced by applied voltage biases has been studied[166,167] by quantifying the frequency of two-level fluctuations (TLF) in conductance of MJs.[166,167] It was found that the frequency of the conductance fluctuations increase with increasing bias and the effective temperature of the MJ is proportional to $\sqrt{V}$ (Fig. 19(b)). Along the same lines, Tsutsui *et al.*[168] reported an estimation of the local temperature by fitting the molecular junction lifetime to a model that takes into consideration both the applied bias and the

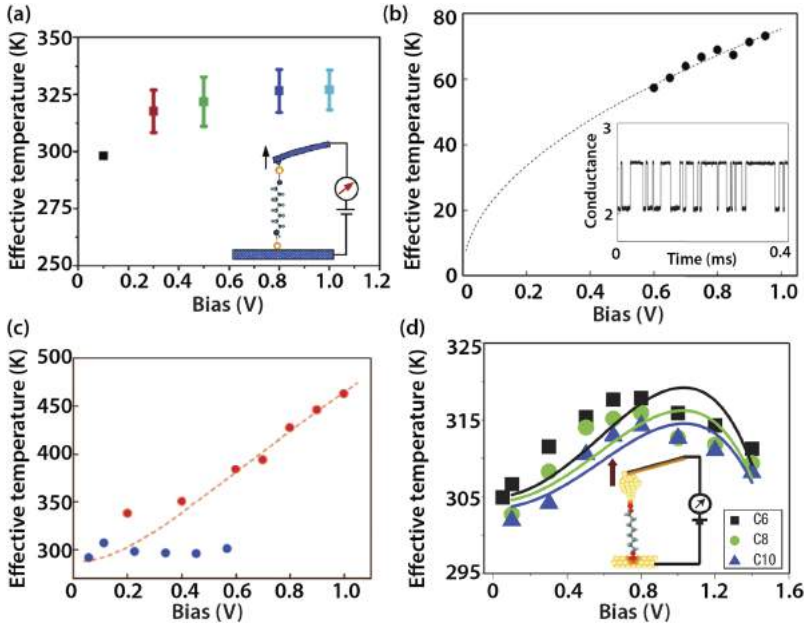

FIG. 19. Measured effective local temperature of MJs. (a) Local temperature of octanedithol under different biases measured by the AFM break junction technique at room temperature.[165] The junction breaking force is directly measured and was used to calculate the local temperature. Reproduced with permission from Huang *et al.*, Nano Lett. **6**, 1240 (2006). Copyright 2006 American Chemical Society. (b) Local temperature ($T_{electrode}$ = 4.2 K) of Au atomic junctions under different biases.[167] The frequency of two-level-fluctuations (TLFs) of conductance was used as an indicator of the local temperature. Reproduced with permission from M. Tsutsui, S. Kurokawa, and A. Sakai, Nanotechnology **17**, 5334 (2006). Copyright 2006 IOP publishing. (c) Local temperature ($T_{electrode}$ = 287 K) of BDT MJ (red) and Au atomic junction (blue).[168] The junction lifetime was used to deduce the local temperature. Reproduced with permission from M. Tsutsui, M. Taniguchi, and T. Kawai, Nano Lett. **8**, 3293 (2008). Copyright 2008 American Chemical Society. (d) Bias dependent local temperature of ADT (N = 6, 8, 10).[170] $T_{electrode}$ = 300 K, and STM break junction technique was used to measure the junction stretching length for estimating the local temperature. Reproduced with permission from Huang *et al.*, Nat. Nanotechnol. **2**, 698 (2007). Copyright 2007 Macmillan Publishers Ltd.

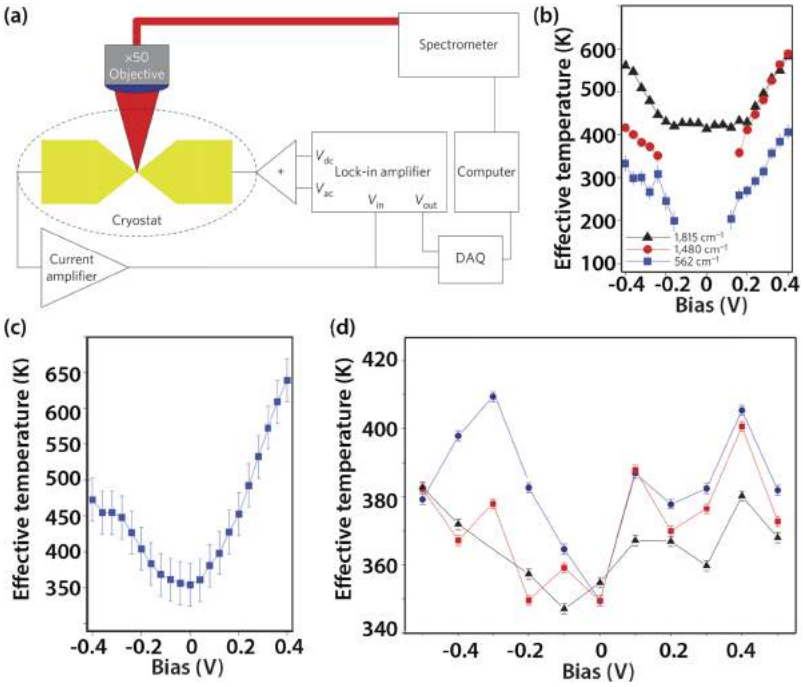

FIG. 20. Local temperature measurements from surface-enhanced Raman spectroscopy. (a) Schematic of the electrical and optical measurements.[172] (b) Bias-dependent phononic effective temperature in OPV3 molecule for different phonon modes.[172] (c) Bias-dependent electronic effective temperature of OPV3 molecule.[172] (a)–(c) reproduced with permission from Ward *et al.*, Nat. Nanotechnol. **6**, 33 (2011). Copyright 2011 Macmillan Publishers Ltd. (d) Phononic effective temperature in BPDT molecule for different phonon modes under different bias voltages.[171] Reproduced with permission from Ioffe *et al.*, Nat. Nanotechnol. **3**, 727 (2008). Copyright 2008 Macmillan Publishers Ltd.

effective temperature. From these studies it was found that Au–BDT–Au molecule junctions were heated up by ~200 K at room temperature under an applied bias of ~1 V (Fig. 19(c)). Further, inelastic electron tunneling spectroscopy[169] (IETS) studies were used to study the onset of heat generation in MJs due to the excitation of the lowest energy phonon mode.

Huang *et al.*[170] also studied the effective temperature of a series of ADT MJs by using the STMBJ technique (Fig. 19(d)). In this work, the stretching lengths of a MJ at breakdown were measured and fitted to a model that describes the dependence of stretching length on effective temperature. They found that the local temperature increases with the applied bias until ~0.8 V and then decreased in the presence of higher biases, suggesting that strong electron-electron scattering led to local ionic cooling. Further, they studied the dependence of effective temperature on the molecular length and found that at a given bias the effective temperature was higher for shorter MJs, indicating that electron-phonon scattering is reduced when MJs were longer.

Besides the measurements of local temperatures using break-junction techniques, Ioffe *et al.*[171] and Ward *et al.*[172] also leveraged surface-enhanced Raman spectroscopy to study this problem (Fig. 20). In their works, the Stokes (S) and anti-Stokes (AS) components of the Raman scattering were measured and the AS/S ratio, which is temperature dependent, was used to estimate the local heating effects. Specifically, Ward *et al.*[172] characterized both the effective vibrational and electronic temperatures of OPV3 molecular junctions and observed a pronounced heating effect with ~200–300 K local temperature increase in the presence of applied bias ~0.4 V. In contrast, Ioffe *et al.*[171] reported a much smaller temperature increase (30–50 K) for the same bias in DBDT MJs. These studies indicate that local Raman spectroscopy may serve as a valuable technique to probe local temperatures at the atomic scale.

In addition to these studies, Schulze *et al.*[173] used a STM to measure heating and heat dissipation processes in single C_{60} molecules. Specifically, they observed the thermally induced decomposition of molecular structures. In the tunneling regime, they found that dissipation of ~20 μW of power was sufficient to cause strong molecule heating and a breakdown of the fullerene cage. In contrast they found that when the molecule was in good contact with both the electrodes, a larger amount of power was necessary for the breakdown of the fullerene cage. Given these observations, they concluded that in the case of junctions with good contact with electrodes either the heat generation in the molecule was less effective or the heat dissipation through phonon-electrode coupling was stronger.

To directly quantify heat dissipation in MJs, Lee *et al.*[174] employed scanning probes that featured a nanoscale thermocouple integrated into the tip of the probe (Fig. 21). By measuring the temperature rise in the tip under positive and negative applied biases, they were able to identify the asymmetric heat dissipation characteristics in the electrodes of the short molecular junctions created with benzenediisonitrile (BDNC) and benzenediamine (BDA) molecules. Similar measurements performed using gold atomic junctions showed no significant asymmetries. The authors combined their measurements of asymmetry with first principle calculations to show that heat dissipation asymmetries were related to the sign and the magnitude of the Seebeck coefficient.[38] Specifically, they concluded that, under an applied bias V, the difference between the heat dissipated in the left electrode (Q_L) and that in the right electrode (Q_R) is given by

$$Q_L(V) - Q_R(V) \approx 2G_eTSV + O(V^3), \tag{11}$$

where S is the Seebeck coefficient of the junction, T is the absolute temperature, and G_e is the electrical conductance of the junctions.

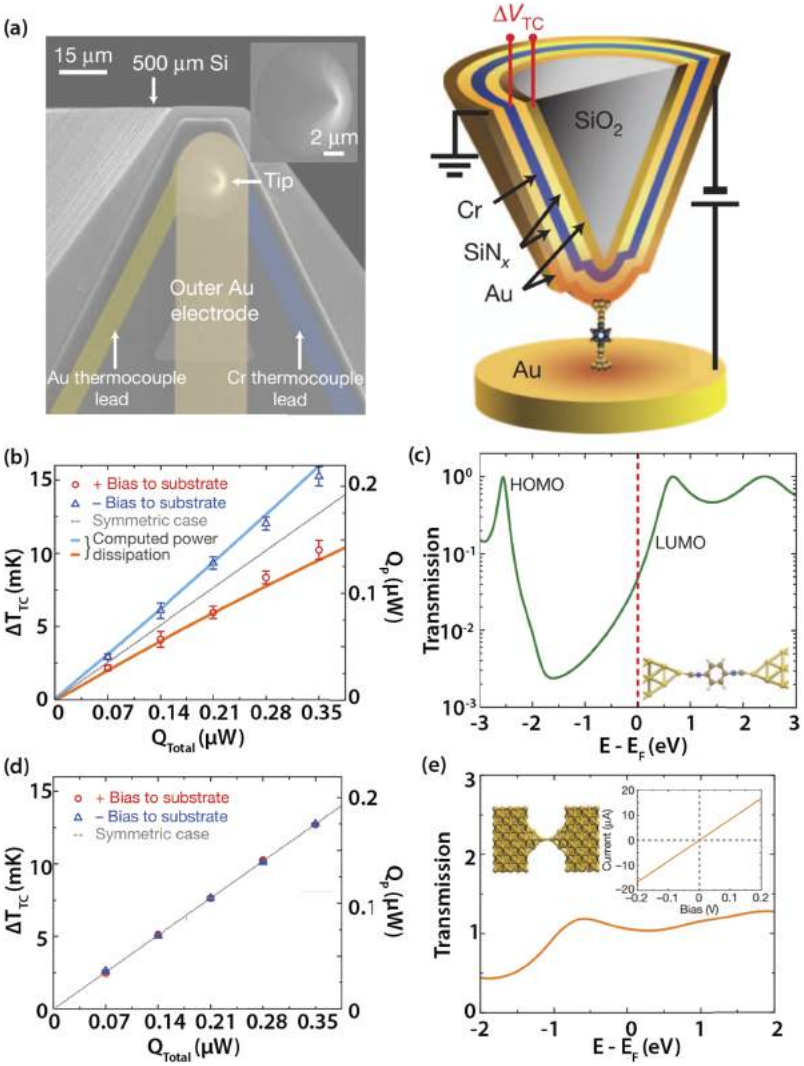

FIG. 21. Direct measurement of the heat dissipation in single atomic and molecular junctions using scanning thermal probes with integrated thermocouple.[174] (a) SEM image (left panel) and schematic (right panel) of the SThM probe featuring an embedded nanoscale thermocouple (Au–Cr) to record the temperature change of the tip due to dissipated heat. (b) Measured asymmetric heat dissipation in the electrodes of a Au-BDNC-Au junction. (c) Calculated transmission function of the Au-BDNC-Au junction. (d) Symmetric heat dissipation observed in the electrodes of Au atomic junctions. (e) Calculated transmission function for Au–Au atomic junctions. Reproduced with permission from Lee *et al.*, Nature **498**, 209 (2013). Copyright 2013 Macmillan Publishers Ltd.

We note that in the experiments discussed above, some were aimed at resolving the inelastic scattering mechanisms in the molecular regions of MJs, while others focused on resolving heat dissipation in the electrodes and assumed that there is negligible dissipation in the molecular regions. These goals do not necessarily contradict each other: as discussed above, the power supplied to sustain the electron flow in MJs must be dissipated in either the electrodes or the molecular region, or both. The heat dissipation in the molecular region of short MJs is usually a very small portion of the total heat dissipation. But even such minute levels of dissipation cause large increases in the local temperature.

V. CONCLUDING REMARKS AND OUTLOOK

Experimental interrogation of thermoelectric energy conversion, heat transport, and heat dissipation in MJs poses several challenges overcoming which is critical to testing current predictions and stimulating future theoretical and computational work. We conclude this review by discussing some outstanding challenges.

A key challenge in thermoelectric energy conversion is to experimentally demonstrate large thermoelectric efficiencies (i.e., ZT values >1) in MJs. While several computations have suggested the feasibility of achieving efficient and/or high power output, thermoelectric energy conversion experiments have so far failed to achieve this goal. Further development of thermoelectric measurements schemes, especially three terminal techniques, may be required to successfully explore the limits of thermoelectric energy conversion in MJs. Moreover, it is also important to explore strategies for developing thermoelectric devices/materials where MJs form the functional subunits.

Probing thermal transport in single MJs and polymer chains is critical for achieving efficient thermoelectric energy conversion and for understanding the physics of heat transfer in these fundamentally different structures. While ensemble based experiments (such as in SAM and polymer nanofibers) have made impressive progress in understanding thermal transport properties, they fail to reveal heterogeneities and can only reveal averaged properties. Single-molecule thermal transport measurement will enable direct comparisons among multiple theories in this field and help build guiding principles for designing MJs for optimal thermal transport.

Recent work by Cui *et al.*[184,185] has shown that it is possible to systematically study heat transfer due to both thermal radiation and conduction at the nanoscale. Specifically, very

recent advances by Cui *et al.*[185] have shown that novel picowatt-resolution scanning calorimetric probes can be employed to measure thermal transport in metallic single-atom junctions. Further, they observed the phenomena of thermal conductance quantization at room temperature. This recent work offers new opportunities to explore thermal transport in molecular junctions, one-dimensional chains of atoms and individual polymer chains, all of which have been studied extensively for over half a century but have not been experimentally accessible.

Another topic of interest is to probe heat dissipation and measuring local temperatures. Existing experimental approaches are not completely capable of resolving the validity of competing theoretical models. To overcome this challenge, high resolution heat dissipation measurements at the single-molecule level are required. Such measurements will enable establishing a precise limit for the fraction of heat dissipation in the molecular region and will play a critical role in verifying the proposed models for heating/cooling of molecules directly.

ACKNOWLEDGMENTS

We acknowledge support from the U.S. Department of Energy Basic Energy Sciences through a grant from the Scanning Probe Microscopy Division under Award No. DE-SC0004871.

[1]A. Aviram and M. A. Ratner, Chem. Phys. Lett. **29**, 277 (1974).
[2]A. Nitzan and M. A. Ratner, Science **300**, 1384 (2003).
[3]N. J. Tao, Nat. Nanotechnol. **1**, 173 (2006).
[4]S. V. Aradhya and L. Venkataraman, Nat. Nanotechnol. **8**, 399 (2013).
[5]D. Xiang *et al.*, Chem. Rev. **116**, 4318 (2016).
[6]F. Chen *et al.*, Annu. Rev. Phys. Chem. **58**, 535 (2007).
[7]L. Sun *et al.*, Chem. Soc. Rev. **43**, 7378 (2014).
[8]R. J. Nichols and S. J. Higgins, Annu. Rev. Anal. Chem. **8**, 389 (2015).
[9]M. Galperin *et al.*, Science **319**, 1056 (2008).
[10]M. Galperin, M. A. Ratner, and A. Nitzan, J. Phys.: Condens. Matter **19**, 103201 (2007).
[11]Y. Dubi and M. Di Ventra, Rev. Mod. Phys. **83**, 131 (2011).
[12]J. P. Bergfield and M. A. Ratner, Phys. Status Solidi B **250**, 2249 (2013).
[13]W. Lee, B. Song, and P. Reddy, Annu. Rev. Heat Transfer **16**, 259 (2013).
[14]L. Rincon-Garcia *et al.*, Chem. Soc. Rev. **45**, 4285 (2016).
[15]D. Segal and B. K. Agarwalla, Annu. Rev. Phys. Chem. **67**, 185 (2016).
[16]J. A. Malen *et al.*, Chem. Phys. Lett. **491**, 109 (2010).
[17]C. M. Finch, V. M. Garcia-Suarez, and C. J. Lambert, Phys. Rev. B **79**, 033405 (2009).
[18]J. P. Bergfield, M. A. Solis, and C. A. Stafford, ACS Nano **4**, 5314 (2010).
[19]N. Nakpathomkun, H. Q. Xu, and H. Linke, Phys. Rev. B **82**, 235428 (2010).
[20]J. Vacek *et al.*, Nanoscale **7**, 8793 (2015).
[21]A. Henry and G. Chen, Phys. Rev. Lett. **101**, 235502 (2008).
[22]J. Liu and R. G. Yang, Phys. Rev. B **86**, 104307 (2012).
[23]R. Landauer, IBM J. Res. Dev. **1**, 223 (1957).
[24]R. Landauer, J. Phys.: Condens. Matter **1**, 8099 (1989).
[25]Y. Imry, *Introduction to Mesoscopic Physics* (Oxford University Press, New York, 1997).
[26]S. Datta, *Quantum Transport: Atom to Transistor* (Cambridge University Press, Cambridge, UK, New York, 2005).
[27]P. N. Butcher, J. Phys.: Condens. Matter **2**, 4869 (1990).
[28]M. Paulsson and S. Datta, Phys. Rev. B **67**, 241403 (2003).
[29]K. Esfarjani, M. Zebarjadi, and Y. Kawazoe, Phys. Rev. B **73**, 085406 (2006).
[30]U. Sivan and Y. Imry, Phys. Rev. B **33**, 551 (1986).
[31]R. Lake and S. Datta, Phys. Rev. B **46**, 4757 (1992).
[32]S. H. Ke *et al.*, Nano Lett. **9**, 1011 (2009).
[33]M. Leijnse, M. R. Wegewijs, and K. Flensberg, Phys. Rev. B **82**, 045412 (2010).
[34]N. R. Claughton and C. J. Lambert, Phys. Rev. B **53**, 6605 (1996).
[35]F. Huser and G. C. Solomon, J. Phys. Chem. C **119**, 14056 (2015).
[36]G. C. Solomon, Nat. Mater. **15**, 254 (2016).
[37]M. Burkle *et al.*, Phys. Rev. B **86**, 115304 (2012).
[38]L. A. Zotti *et al.*, New J. Phys. **16**, 015004 (2014).
[39]F. Pauly *et al.*, Phys. Rev. B **84**, 195420 (2011).
[40]M. Burkle *et al.*, Phys. Rev. B **91**, 165419 (2015).
[41]J. P. Bergfield and C. A. Stafford, Nano Lett. **9**, 3072 (2009).
[42]Z. H. Wang *et al.*, Science **317**, 787 (2007).
[43]G. D. Mahan and J. O. Sofo, Proc. Natl. Acad. Sci. U. S. A. **93**, 7436 (1996).
[44]O. Karlstrom *et al.*, Phys. Rev. B **84**, 113415 (2011).
[45]D. Nozaki *et al.*, Phys. Rev. B **81**, 235406 (2010).
[46]A. E. Miroshnichenko, S. Flach, and Y. S. Kivshar, Rev. Mod. Phys. **82**, 2257 (2010).
[47]D. Bohm, *Quantum Theory* (Prentice-Hall, New York, 1951).
[48]C. J. Lambert, Chem. Soc. Rev. **44**, 875 (2015).
[49]M. Bernien *et al.*, J. Phys. Chem. Lett. **3**, 3431 (2012).
[50]B. Warner *et al.*, J. Phys. Chem. Lett. **4**, 1546 (2013).
[51]D. Aravena and E. Ruiz, J. Am. Chem. Soc. **134**, 777 (2012).
[52]D. Ghosh, P. Parida, and S. K. Pati, Appl. Phys. Lett. **106**, 193105 (2015).
[53]R. S. Whitney, Phys. Rev. Lett. **112**, 130601 (2014).
[54]R. S. Whitney, Phys. Rev. B **91**, 115425 (2015).
[55]C. J. Lambert, H. Sadeghi, and Q. H. Al-Galiby, C. R. Phys. **17**, 1084 (2016).
[56]V. M. Garcia-Suarez *et al.*, Nanotechnology **25**, 205402 (2014).
[57]Q. H. Al-Galiby *et al.*, Nanoscale **8**, 2428 (2016).
[58]H. Sadeghi, S. Sangtarash, and C. J. Lambert, Beilstein J. Nanotechnol. **6**, 1413 (2015).
[59]P. Reddy *et al.*, Science **315**, 1568 (2007).
[60]B. Q. Xu and N. J. Tao, Science **301**, 1221 (2003).
[61]W. Lee and P. Reddy, Nanotechnology **22**, 485703 (2011).
[62]J. R. Widawsky *et al.*, Nano Lett. **12**, 354 (2012).
[63]A. Tan, S. Sadat, and P. Reddy, Appl. Phys. Lett. **96**, 013110 (2010).
[64]J. Moreland and J. W. Ekin, J. Appl. Phys. **58**, 3888 (1985).
[65]C. J. Muller, J. M. Vanruitenbeek, and L. J. Dejongh, Phys. Rev. Lett. **69**, 140 (1992).
[66]A. I. Yanson *et al.*, Nature **395**, 783 (1998).
[67]B. Ludoph and J. M. van Ruitenbeek, Phys. Rev. B **59**, 12290 (1999).
[68]R. H. Smit *et al.*, Nature **419**, 906 (2002).
[69]N. Agrait, A. L. Yeyati, and J. M. van Ruitenbeek, Phys. Rep. **377**, 81 (2003).
[70]R. H. M. Smit, C. Untiedt, and J. M. van Ruitenbeek, Nanotechnology **15**, S472 (2004).
[71]C. A. Martin, J. M. van Ruitenbeek, and H. S. J. van der Zant, Nanotechnology **21**, 265201 (2010).
[72]D. Xiang *et al.*, Adv. Mater. **25**, 4845 (2013).
[73]M. A. Reed *et al.*, Science **278**, 252 (1997).
[74]M. Tsutsui *et al.*, Sci. Rep. **5**, 11519 (2015).
[75]J. A. Malen *et al.*, Nano Lett. **9**, 1164 (2009).
[76]J. A. Malen *et al.*, Nano Lett. **9**, 3406 (2009).
[77]J. R. Widawsky *et al.*, Nano Lett. **13**, 2889 (2013).
[78]E. Macia, Phys. Rev. B **75**, 035130 (2007).
[79]Y. Q. Li *et al.*, Nat. Commun. **7**, 11294 (2016).
[80]C. Evangeli *et al.*, Nano Lett. **13**, 2141 (2013).
[81]Y. Q. Xue and M. A. Ratner, Phys. Rev. B **69**, 085403 (2004).
[82]J. Balachandran *et al.*, J. Phys. Chem. Lett. **4**, 3825 (2013).
[83]J. Balachandran *et al.*, J. Phys. Chem. Lett. **3**, 1962 (2012).
[84]S. Bilan *et al.*, Phys. Rev. B **85**, 205403 (2012).
[85]A. Tan *et al.*, J. Am. Chem. Soc. **133**, 8838 (2011).
[86]K. Baheti *et al.*, Nano Lett. **8**, 715 (2008).
[87]L. Venkataraman *et al.*, Nature **442**, 904 (2006).
[88]A. Mishchenko *et al.*, Nano Lett. **10**, 156 (2010).
[89]K. Wang *et al.*, Chem. Sci. **5**, 3425 (2014).
[90]S. K. Lee *et al.*, Nanoscale **7**, 20497 (2015).
[91]L. Rincon-Garcia *et al.*, Nat. Mater. **15**, 289 (2016).
[92]C. Evangeli *et al.*, Nano Lett. **15**, 1006 (2015).
[93]E. Zerah-Harush and Y. Dubi, Phys. Rev. Appl. **3**, 064017 (2015).
[94]J. M. Beebe *et al.*, J. Am. Chem. Soc. **124**, 11268 (2002).
[95]S. N. Yaliraki, M. Kemp, and M. A. Ratner, J. Am. Chem. Soc. **121**, 3428 (1999).
[96]S. K. Yee *et al.*, Nano Lett. **11**, 4089 (2011).
[97]S. K. Lee *et al.*, Nano Lett. **14**, 5276 (2014).
[98]Y. Kim *et al.*, Appl. Phys. Lett. **109**, 033102 (2016).

[99]A. R. Champagne, A. N. Pasupathy, and D. C. Ralph, Nano Lett. **5**, 305 (2005).
[100]E. A. Osorio *et al.*, J. Phys.: Condens. Matter **20**, 374121 (2008).
[101]D. Xiang *et al.*, Nano Lett. **13**, 2809 (2013).
[102]H. Song *et al.*, Nature **462**, 1039 (2009).
[103]H. Park *et al.*, Appl. Phys. Lett. **75**, 301 (1999).
[104]J. Park *et al.*, Nature **417**, 722 (2002).
[105]J. Maeng *et al.*, Appl. Phys. Lett. **92**, 233120 (2008).
[106]E. A. Osorio *et al.*, Nano Lett. **10**, 105 (2010).
[107]A. Javey *et al.*, Nat. Mater. **1**, 241 (2002).
[108]N. M. Gabor *et al.*, Science **325**, 1367 (2009).
[109]P. Jarillo-Herrero *et al.*, Nature **434**, 484 (2005).
[110]W. Jeong *et al.*, Sci. Rep. **4**, 4975 (2014).
[111]Y. Kim *et al.*, Nat. Nanotechnol. **9**, 881 (2014).
[112]E. Fermi, J. Pasta, and S. Ulam, Los Alamos Report LA-1940 978, 1955.
[113]S. Lepri, R. Livi, and A. Politi, Phys. Rep. **377**, 1 (2003).
[114]A. Dhar, Adv. Phys. **57**, 457 (2008).
[115]D. Segal, A. Nitzan, and P. Hanggi, J. Chem. Phys. **119**, 6840 (2003).
[116]H. Sadeghi, S. Sangtarash, and C. J. Lambert, Nano Lett. **15**, 7467 (2015).
[117]J. C. Klockner *et al.*, Phys. Rev. B **94**, 205425 (2016).
[118]T. Markussen, J. Chem. Phys. **139**, 244101 (2013).
[119]C. M. Guedon *et al.*, Nat. Nanotechnol. **7**, 305 (2012).
[120]T. F. Luo and J. R. Lloyd, Int. J. Heat Mass Transfer **53**, 1 (2010).
[121]T. F. Luo and J. R. Lloyd, J. Appl. Phys. **109**, 034301 (2011).
[122]T. F. Luo and J. R. Lloyd, J. Heat Transfer **132**, 032401 (2010).
[123]J. C. Duda *et al.*, J. Chem. Phys. **134**, 094704 (2011).
[124]J. V. Goicochea *et al.*, J. Heat Transfer **133**, 082401 (2011).
[125]L. Hu *et al.*, Phys. Rev. B **81**, 235427 (2010).
[126]N. B. Li *et al.*, Rev. Mod. Phys. **84**, 1045 (2012).
[127]D. Segal and A. Nitzan, Phys. Rev. Lett. **94**, 034301 (2005).
[128]D. Segal and A. Nitzan, J. Chem. Phys. **122**, 194704 (2005).
[129]D. Segal, Phys. Rev. B **73**, 205415 (2006).
[130]E. Diaz, R. Gutierrez, and G. Cuniberti, Phys. Rev. B **84**, 144302 (2011).
[131]M. G. Menezes *et al.*, Phys. Rev. B **81**, 012302 (2010).
[132]Q. Li *et al.*, J. Phys. Chem. C **119**, 24636 (2015).
[133]J. Ren, P. Hanggi, and B. W. Li, Phys. Rev. Lett. **104**, 170601 (2010).
[134]F. Zhan *et al.*, Phys. Rev. E **80**, 061115 (2009).
[135]C. L. Choy, Polymer **18**, 984 (1977).
[136]J. J. Freeman, G. J. Morgan, and C. A. Cullen, Phys. Rev. B **35**, 7627 (1987).
[137]A. Henry and G. Chen, Phys. Rev. B **79**, 144305 (2009).
[138]K. Sasikumar and P. Keblinski, J. Appl. Phys. **109**, 114307 (2011).
[139]R. Y. Wang, R. A. Segalman, and A. Majumdar, Appl. Phys. Lett. **89**, 173113 (2006).
[140]G. Kirsanskas *et al.*, Appl. Phys. Lett. **105**, 233102 (2014).
[141]J. C. Love *et al.*, Chem. Rev. **105**, 1103 (2005).
[142]Z. B. Ge, D. G. Cahill, and P. V. Braun, Phys. Rev. Lett. **96**, 186101 (2006).
[143]C. A. Paddock and G. L. Eesley, J. Appl. Phys. **60**, 285 (1986).
[144]Z. T. Tian, A. Marconnet, and G. Chen, Appl. Phys. Lett. **106**, 211602 (2015).
[145]D. G. Cahill, Rev. Sci. Instrum. **61**, 802 (1990).
[146]P. J. O'Brien *et al.*, Nat. Mater. **12**, 118 (2013).
[147]M. D. Losego *et al.*, Nat. Mater. **11**, 502 (2012).
[148]S. Majumdar *et al.*, Nano Lett. **15**, 2985 (2015).
[149]A. J. Schmidt, R. Cheaito, and M. Chiesa, Rev. Sci. Instrum. **80**, 094901 (2009).
[150]T. Meier *et al.*, Phys. Rev. Lett. **113**, 060801 (2014).
[151]S. Shen *et al.*, Nat. Nanotechnol. **5**, 251 (2010).
[152]X. J. Wang *et al.*, Macromolecules **46**, 4937 (2013).
[153]J. Ma *et al.*, Nanoscale **7**, 16899 (2015).
[154]D. Segal and A. Nitzan, J. Chem. Phys. **117**, 3915 (2002).
[155]A. Pecchia, G. Romano, and A. Di Carlo, Phys. Rev. B **75**, 035401 (2007).
[156]M. Galperin, A. Nitzan, and M. A. Ratner, Phys. Rev. B **75**, 155312 (2007).
[157]R. D'Agosta, N. Sai, and M. Di Ventra, Nano Lett. **6**, 2935 (2006).
[158]Z. Yang *et al.*, Phys. Rev. B **71**, 041402 (2005).
[159]Y. C. Chen, M. Zwolak, and M. Di Ventra, Nano Lett. **5**, 621 (2005).
[160]M. Galperin *et al.*, Phys. Rev. B **80**, 115427 (2009).
[161]G. Romano *et al.*, Phys. Rev. B **81**, 115438 (2010).
[162]R. Hartle and M. Thoss, Phys. Rev. B **83**, 115414 (2011).
[163]L. Simine and D. Segal, Phys. Chem. Chem. Phys. **14**, 13820 (2012).
[164]J. Lykkebo *et al.*, J. Chem. Phys. **144**, 114310 (2016).
[165]Z. F. Huang *et al.*, Nano Lett. **6**, 1240 (2006).
[166]M. Tsutsui *et al.*, Jpn. J. Appl. Phys., Part 1 **44**, 5188 (2005).
[167]M. Tsutsui, S. Kurokawa, and A. Sakai, Nanotechnology **17**, 5334 (2006).
[168]M. Tsutsui, M. Taniguchi, and T. Kawai, Nano Lett. **8**, 3293 (2008).
[169]M. A. Reed, Mater. Today **11**, 46 (2008).
[170]Z. F. Huang *et al.*, Nat. Nanotechnol. **2**, 698 (2007).
[171]Z. Ioffe *et al.*, Nat. Nanotechnol. **3**, 727 (2008).
[172]D. R. Ward *et al.*, Nat. Nanotechnol. **6**, 33 (2011).
[173]G. Schulze *et al.*, Phys. Rev. Lett. **100**, 136801 (2008).
[174]W. Lee *et al.*, Nature **498**, 209 (2013).
[175]J. C. Klöckner *et al.*, e-print arXiv:1609.03827 (2016).
[176]T. Morikawa *et al.*, Nanoscale **6**, 8235 (2014).
[177]S. Kaneko *et al.*, Appl. Phys. Express **8**, 095503 (2015).
[178]W. B. Chang *et al.*, Phys. Chem. Chem. Phys. **17**, 6207 (2015).
[179]D. Kim, P. S. Yoo, and T. Kim, J. Korean Phys. Soc. **66**, 602 (2015).
[180]T. Kim *et al.*, Nano Lett. **14**, 794 (2014).
[181]S. Y. Guo, G. Zhou, and N. J. Tao, Nano Lett. **13**, 4326 (2013).
[182]W. B. Chang *et al.*, Chem. Mater. **26**, 7229 (2014).
[183]E. J. Dell *et al.*, Nat. Chem. **7**, 209 (2015).
[184]L. Cui *et al.*, Nat. Commun. **8**, 14479 (2017).
[185]L. Cui *et al.*, "Quantized thermal transport in single-atom junctions," Science (published online).